STATISTICS, OPTIMIZATION AND INFORMATION COMPUTING
Stat., Optim. Inf. Comput., Vol. **15**, January 2026, pp 646–682.
Published online in International Academic Press (www.IAPress.org)

Third Harmonic Injection Reference with Edge Shifted Carriers to Three-Phase Inverter-Fed Induction Motor

Bhavana Kadiyala[1,*], R. Bensraj[1], P.Muthukumar[2]

[1] *Department of Electrical Engineering, Annamalai University, Chidambaram, Tamilnadu, India*
[2] *Department of Electrical and Electronic Engineering, Saveetha School of Engineering, Saveetha Institute of Medical and Technical Sciences, Chennai, Tamil Nadu*

Abstract A three-phase induction motor (IM) fed by an inverter is widely used in industrial and commercial drives because it can effectively convert Direct Current (DC) power to balanced three-phase alternating current (AC) power, which is suitable for driving IMs. Pulse Width Modulation (PWM) switching introduces harmonics into the output voltage, which can cause additional heating of the motor, torque ripple, and electromagnetic interference (EMI). This research investigates the design and performance improvement of a three-phase Voltage Source Inverter (VSI) system for effective IM operation, combined with a new Kookaburra-based Modular Neural Control Framework (KbMNCF). The first step is designing a conventional VSI topology using a DC voltage source, power electronic switches, and PWM to convert the DC input into a balanced three-phase AC output for industrial motor drives. To maximize inverter performance while adapting the control, the introduced KbMNCF is used to tune the PWM parameters. The PWM techniques adopted include Third Harmonic Injection (THI) for maximizing the output voltage and an Edge-Shifted Carrier (ESC) method for allocating switching actions, thereby minimizing switching losses and thermal stress. The system's overall robustness is confirmed by assessing key performance metrics, including Total Harmonic Distortion (THD), Voltage, and system efficiency. Simulation and analysis have demonstrated significant improvements in waveform quality, torque smoothness, and energy efficiency, thereby verifying the validity of the proposed control framework for high-performance inverter-fed motor drives.

Keywords Three Phase Inverter, Third Harmonic Injection, Voltage, Total Harmonic Distortion.

AMS 2010 subject classifications 62M10, 93A30

DOI: 10.19139/soic-2310-5070-2703

1. Introduction

Front-end converters with three-phase diode rectifiers are widely used in AC–AC power conversion schemes, such as adjustable speed AC Drives (ASDs) and uninterruptible power supplies, due to their desirable characteristics, including low cost, a reliable and straightforward configuration, high efficiency, and low electromagnetic interference noise [1]. However, the highly distorted line current of diode rectifier front-end converters is one of its undesirable features, which may result in harmonic pollution of the power system [2]. For the first solution, there are two standard active PFC converters: voltage-source-type back-to-back PWM conversions (C-BBC) and source-type back-to-back PWM conversions (V-BBC) [3]. Bidirectional power flow, sinusoidal input currents, and variable input power factors are among its advantageous characteristics [4]. However, the large and significant energy storage components in the DC-link limit the compactness and network integration of the converter [5]. Alternatively, matrix conversions (MCs) can be used, which have gained popularity in recent times since they do not require energy storage devices [6]. MCs can be classified into two groups: direct matrix converters (DMCs)

*Correspondence to: Bhavana Kadiyala (Email: bhavana.kadiyala1@gmail.com). Department of Electrical Engineering, Annamalai University, Chidambaram, Tamil Nadu, India.

ISSN 2310-5070 (online) ISSN 2311-004X (print)

or inverse matrix converters (IMCs) [7]. Another topology of the V-BBC is the matrix converter (MC), which has become increasingly popular over the past decade due to its enhanced reliability and lack of energy storage elements [8][9]. In contrast to the DMC, the IMC features zero-current modulation and a simpler clamping circuit for preventing excessive voltage [10].

However, in most industrial applications, such as steel processing, unwinding-rewinding production, diesel-electric locomotion, more electric aircraft, and offshore ship propulsion, there is a need for single feeding of multiple three phase loads [11]. Additionally, the effective DC link of the IMC makes it more scalable, thus making it potentially suitable for these particular applications [12]. However, the drawback of the two topologies is their high switch capacity in addition to inefficient utilisation of the DC-link voltage [13]. Additionally, the topology, which involves many three-phase VSIs with a shared rectifier, is also constrained by a high computational load due to the rigid modulation synchronisation between the inverter and rectifier, especially when the VSIs are extremely large in Number [14]. For MCs, unity input power factor conditions are typically more desirable [15]. MCs require input reactive power in specific applications, such as wind energy conversion systems [16]. By altering the intended displacement angle, conventional modulation may substantially regulate the input reactive force of IMCs [17]. Unfortunately, with a decreased input power factor, the offered maximum voltage transfer ratio reduces [18]. This is a particularly harsh restriction when the motor supply is limited due to its low output [19].

To enhance converter efficiency, the THI has been controlled by recirculating power in the third harmonics channel back to the DC link through a three-phase boost rectifier [20]. The third harmonic flow in the injection path can be easily regulated using this method, making it suitable for unregulated rectifiers [21]. However, because the firing angle of the three-phase controlled converter differs, it is unable to control the angle of the injection current, which should shift [22]. The innovative approach presented in this work overcame this constraint by controlling the phase angle and amplitude of the injection current through adjustments to the power angle and modulation index of the three-phase PWM converter in the injection branch, respectively [23]. Therefore, this paper presents an innovative approach that integrates the THI reference with edge-shifted carriers to develop a three-phase inverter-fed induction motor (IM).

The key contribution of this current work is described as follows,

- Initially, a three-phase VSI is designed with a DC voltage source, power electronic switches, diodes, a PWM controller, and an IM, among other components, to convert a DC input into a balanced three-phase AC output, which is suitable for driving an IM efficiently.
- Subsequently, a new novel Kookaburra-based Modular Neural Control Framework (KbMNCF) is established in this study to tune PWM parameters for optimal inverter performance adaptively.
- Following that, PWM techniques were employed to generate precise gate signals for inverter switches, enabling effective control of output voltage waveforms.
- A third harmonic component was incorporated into the modulation reference to increase output voltage utilization and significantly reduce THD.
- Introduced an edge-shifted carrier technique to distribute switching events across all three phases (S, T, and V), effectively reducing switching losses and improving thermal balance among inverter legs.
- Finally, the robustness of the suggested technique is evaluated in terms of Voltage, system efficiency, and harmonic distortion reduction.

A recent related study is included in the second part of this paper, and the system's challenges are described in the third. The fourth section provides a detailed explanation of the proposed methodology, and the fifth section presents the performance evaluation of the suggested model. The work is completed in Section 6.

2. Related Works

To following are some recently related literary works,

Current research is focused on PWM strategies that are less stressful on drive units. Demarcus et al. [24] examine carrier-based PWM techniques and propose innovative insights for determining the factor of harmonic Distortion (HD) in an ADTP configuration, contributing to the improvement of theoretical harmonic distortion cancellation

analysis and the accuracy of harmonic profiles. Additionally, it does not examine the thermal or efficiency effects of the proposed PWM methodologies for ADTP drive units.

In this paper, Wang et al. [25] employed space vector methods to systematically evaluate the current harmonic performance of dual three-phase electrical machines. It includes dead-time correction and proposes five different switching sequences, along with their corresponding ideal operating regions. Experimental and simulation results are employed to verify the evaluation. Additionally, the impact of parameter mismatches and system anomalies has not been extensively explored.

Minimising high-frequency harmonics and vibrations is the primary objective of the various random space vector pulse-width modulation (VR-SVPW) methods proposed by Zhao et al. [26] for synchronous dual three-phase magnet machines. The carrier frequency is synthesised by the normal variable time delay SVPWM method, and the modulation interval is 2N. The MR-SVPW method lessens high-frequency harmonics and vibration by integrating traditional random frequency carrier PWM with 2N-period modulated variable delayed time SVPWM. Additionally, its effectiveness under various machine operating conditions has not been extensively evaluated.

VSI-fed permanent synchronous motor drives using magnets must have no current harmonics on either the AC side or the DC side. This paper discusses a method for minimising high-frequency current harmonics on both sides, known as hybrid-frequency phase-shift pulse-width modulation (HFPSPWM). Fu et al. [27] provide an analysis of how phase-shift modulation minimises the root mean square of DC-side current harmonics. Through simulation and experiment, the suggested HFPSPWM is confirmed to minimise the DC-side current harmonics and harmonic Distortion of load currents. Also, the long-term dependability under varying load conditions is not considered.

In this research, Hu et al. [28] discuss common-mode electromagnetic interference (EMI) suppression methods for inverter-fed motor drives. It considers suppression paths and mitigation from sources. Although power device switch transients affect high-frequency EMI, zero common-mode control can reduce low-frequency EMI. To improve switching behaviour, a range of drive circuits is discussed, and active and active and passive filters for compensation or suppression are addressed. Furthermore, the correlation between EMI suppression techniques and motor control efficiency has not been extensively investigated.

Several complementary directions have been identified by recent research on PWM techniques for inverter-fed drives, each with trade-offs that are pertinent to the design of a KbMNCF. First, due to their ability to provide low harmonic Distortion and good DC-bus utilisation, SVPWM and its multilevel variants continue to be a dominant and well-understood family. Recent reviews highlight efforts to reduce low-order harmonics and common-mode voltage, while summarising developments in symmetrical and optimised SVPWM for multilevel and T-type topologies [11]. Second, Third-Harmonic Injection (THI) techniques are still being researched as an economical means of increasing fundamental Voltage and lowering THD. For example, new THI formulations for grid and transmission problems show that they can be used for purposes other than just Voltage boosting, such as transmission uprating and dead time compensation [12]. It has been demonstrated that per-phase randomisation and variable switching-frequency schemes significantly reduce peak emissions, albeit at the expense of increased complexity in filtering and feedback design [3]. Randomised or spread-spectrum PWM techniques also break switching periodicity to smear harmonic energy and reduce EMI. Fourth, combining metaheuristic optimisation (e.g. GA, PSO, GWO) with sophisticated PWM schemes is becoming increasingly popular. In these schemes, carriers, phase shifts, and harmonic injection amplitudes are adjusted for application-specific goals like lowering switching losses, THD, or thermal stress [4]. Finally, frameworks such as KbMNCF for modular neural PWM tuning are directly motivated by the introduction of adaptive neural and predictive controllers for online PWM parameter adaptation, which provide robustness under non-ideal grid or load conditions. Recent work demonstrates their use in sensorless and UPQC-style applications [5, 6].

Research gap

While each of the current PWM techniques for inverter-fed drives has significant advantages, they also have significant drawbacks. Space Vector PWM (SVPWM) and its multilayer expansions lower low-order harmonics and increase DC-bus utilisation, but they also increase switching stress at high frequencies. They are prone to producing large amounts of common-mode Voltage. Although Third Harmonic Injection (THI) techniques effectively raise the fundamental Voltage and reduce some harmonics, they are not flexible enough to handle dynamic loads and grid fluctuations, which frequently leads to decreased performance in real-time operation.

Although randomised and metaheuristic-tuned PWM approaches facilitate the distribution of harmonic energy and reduction of electromagnetic interference, they also present challenges for real-time hardware deployment, increased computational overhead, and unexpected spectral behaviour. This trade-off highlights a research gap: a framework is needed that maintains stability and computational efficiency while minimising harmonic Distortion and effectively utilising Voltage. This is addressed by the suggested Kookaburra-based Modular Neural Control Framework (KbMNCF) with THI-ESC, which adaptively adjusts PWM parameters online to provide inverter-fed induction motor drives with robust harmonic suppression, increased efficiency, and dependable operation.

3. Problem Statement

Conventional sinusoidal PWM techniques are utilised in three-phase inverter-fed IM drives. Additionally, it tends to yield low DC bus voltage utilisation and high harmonic Distortion, which restricts the system's efficiency and performance. These techniques do not correctly handle the harmonic content of the inverter output, thereby reducing power quality and increasing stress on the motor windings. Apart from this, conventional methods are unable to utilise the entire modulating range, resulting in a low output voltage and poor motor performance. In this paper, an attempt has been made to overcome these limitations by utilising THI, edge-shifted carriers, enhanced voltage utilisation, and reducing the harmonic Distortion of the inverter output to a great extent.

This research aims to improve the efficiency of three-phase inverter-driven IM drives by optimising voltage utilisation and reducing harmonic Distortion. The method proposed combines THI with edge-shifted carrier-based PWM schemes to produce superior-quality output voltage waveforms. Traditional sinusoidal PWM systems, although common, fail to utilise the entire DC bus voltage effectively, introducing unwanted harmonics that degrade motor performance. This study addresses a weakness by proposing a superior modulation method to enhance the quality of the inverter output.

4. Proposed Methodology

A novel Kookaburra-based Modular Neural Control Framework (KbMNCF) is established to tune PWM parameters for adaptively optimal inverter performance. Initially, a three-phase VSI is designed with a DC voltage source, power electronic switches, diodes, a PWM controller, and an IM, among other components, to convert a DC input into a balanced three-phase AC output suitable for driving an IM efficiently.

Subsequently, a PWM technique was employed to generate precise gate signals for inverter switches, enabling effective control of output voltage waveforms. It incorporated a third harmonic component into the modulation reference to increase output voltage utilisation and significantly reduce THD. Introduced an edge-shifted carrier technique to distribute switching events across all three phases, effectively reducing switching losses and improving thermal balance among inverter legs. Finally, the robustness of the proposed method is evaluated in terms of voltage utilisation and THD. The proposed architecture is illustrated in Figure 1.

4.1. Process of the proposed KbMNCF

The initial stage in the process was designing a three-phase VSI, which is primarily responsible for transforming a DC input into a balanced three-phase AC output that can efficiently power an IM. A DC voltage source, power electronic switches, drifting diodes, and a pulse width modulator processor are all essential components of the inverter's basic design. It is formulated in Eqn. (1).

$$S_{Ti} = B_x + Gc + Zs + Lk + Sdc \tag{1}$$

Here, the power electronics B_x Gc are the drifting diodes, Zs which are the pulse with the modulator, Lk denotes the basic line-to-line output voltage's RMS value, S_{dc} signifies the DC voltage input for the inverter. The inverter, which transforms DC into balanced three-phase AC through PWM-controlled switches, is powered by a DC voltage source. To ensure that IMs operate efficiently, the output voltage is controlled by the modulation index, and the

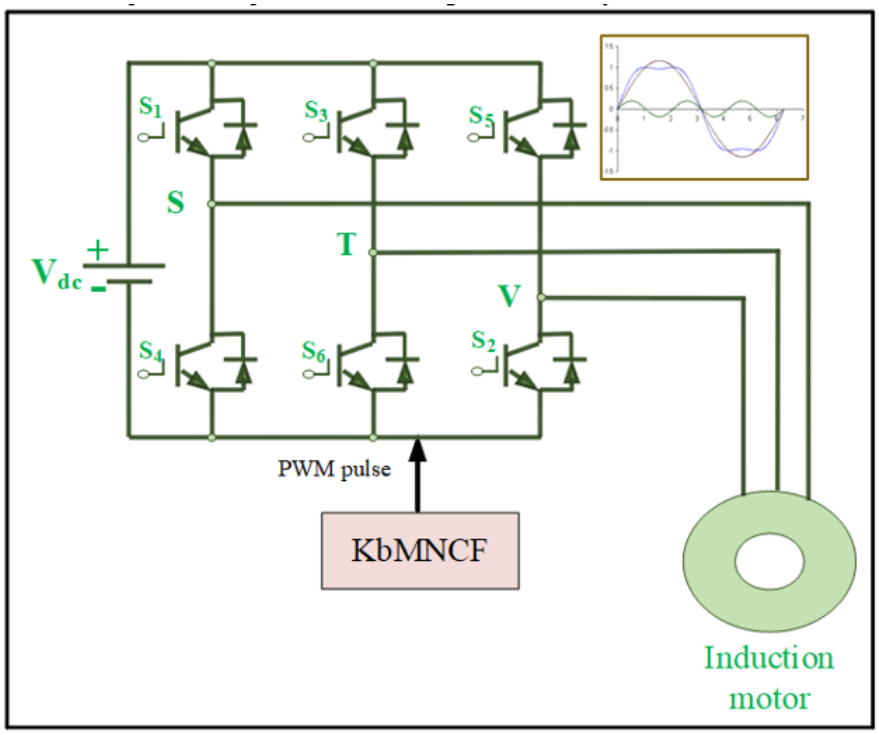

Figure 1. Proposed Architecture

line-to-line Voltage is obtained by multiplying by $\sqrt{3}$. The PWM technique was employed to provide precise gate impulses for the power switches, thereby accurately controlling the inverter's output. PWM regulates the effective Voltage and frequency supplied to the motor by adjusting the pulse width in the switching signals. This modulation technique produces a synthesised output waveform that closely resembles a sinusoidal AC waveform, which is necessary to maintain a smooth motor drive and minimise electrical losses. The motor speed and torque can be dynamically controlled by adjusting the modulation index, providing efficient motor drive control. It is expressed in Eqn. (2).

$$A = \frac{M_{ref}}{M_{carrier}} \tag{2}$$

Here, A denotes the modulation index, m_{ref} signifies the peak of the sinusoidal modulating waveform, and $M_{carrier}$ denotes the peak of the triangular waveform.

$$W(v) = \begin{cases} 0 & \text{if } M_{ref}(v) > M_{carrier}(v) \\ 1 & \text{otherwise} \end{cases} \tag{3}$$

To further improve the performance of the inverter, a third harmonic component was added to the sinusoidal reference signal used for PWM. The method is termed THIPWM. It involves the addition of a calculated third harmonic component to the reference waveform without interfering with the line-to-line voltages, as the third harmonics are cancelled out in a three-phase balanced system. Incorporating this component raises the modulation index above the linear value, enabling more efficient utilisation of the DC bus voltage. Consequently, the output voltage amplitude is increased without raising the DC link voltage, thereby improving voltage utilisation and motor drive efficiency. It is formulated in Eqn. (4).

$$M_{ref}(l) = Ha * \sin(vl) + Ha_d * \sin(3vl) \tag{4}$$

Here, $M_{ref}(l)$ represents the PWM's modified reference signal, Ha denotes the amplitude of the fundamental sinusoidal component, Ha_d represents the amplitude of the THI, υ signifies the fundamental signal's angular frequency, and $\sin(3\upsilon l)$ represents the amplitude of the third harmonic. The modulation index in SPWM is maintained at 1.0 to prevent exceeding the carrier peak. By flattening the reference waveform with the inclusion of a third harmonic, the modulation index can rise over 1.0. Raising the output voltage without overmodulation increases the inverter's efficiency.

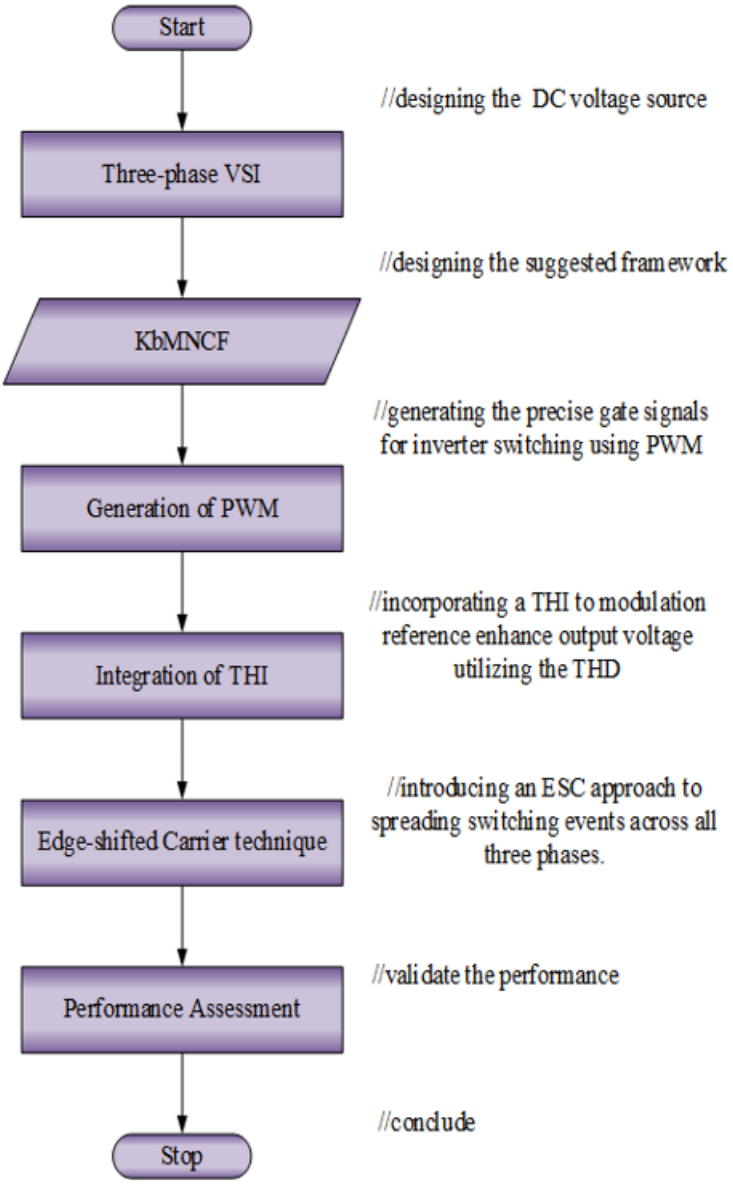

Figure 2. Flow work of KbMNCF

An edge-shifted carrier approach was employed to minimise switching losses and promote thermal balance between the inverter legs. With this method, the triangle carrier waveforms used to compare the modulating signals in each phase leg are phase-shifted in relation to one another. Distributing switching instants throughout the three

inverter legs (S, T, and V) prevents simultaneous switching occurrences and lowers the DC source's peak current demand. As a result, the power electronic switches are more reliable and have a longer lifespan since switching losses are reduced and heat stress is more uniformly distributed among the inverter components. It is expressed in Eqn. (5), (6), and (7).

$$D_{tri,R}(l) = D_{tri}(l) \tag{5}$$

$$D_{tri,S}(l) = D_{tri}(l - \frac{L_u}{3}) \tag{6}$$

$$D_{tri,Q}(l) = D_{tri}(l - \frac{2L_u}{3}) \tag{7}$$

Here, D_{tri}, R, D_{tri}, S and D_{tri}, Q represent the triangular carrier waveforms for phases R S and Q L_u denotes the switching period. Using the same carrier waveform through both inverter legs in conventional PWM may result in simultaneous switching, which increases electromagnetic interference (EMI), causes localised heating, and leads to significant switching losses. The manuscript's introduction of the idea of edge-shifted carriers lacks standardization and clarity. According to Eqn. (5)-(7), the method is equivalent to a 120° phase shift between the triangular carrier signals, which is consistent with the widely used Phase-Shifted Carriers (PSC) technique. PSC is frequently used in multilevel converters and parallel inverters to distribute thermal stress among switching devices efficiently, reduce current ripple, and increase the apparent switching frequency. Edge-shifting is a concept that requires definition. Adopting the standard PSC language would provide clarity and consistency with the published literature. If the suggested approach is meant to represent a modification of conventional PSC, its unique contribution and justification should be explicitly noted.

The switching instants in a traditional two-level three-phase voltage source inverter (VSI) occur concurrently across phases, as all three legs typically employ the same triangular carrier waveform. Large instantaneous current spikes in the DC connection, concentrated switching losses, and increased thermal stress on the semiconductor devices are the outcomes of this coordinated action. Phase-shifted carriers (PSC), on the other hand, stagger the switching transitions over the basic cycle by shifting the carriers for each phase leg by 120°. In addition to distributing switching losses more evenly among the devices and reducing peak current demand on the DC bus, this staggering minimises the likelihood of simultaneous switching events. Consequently, PSC helps reduce electromagnetic interference (EMI), enhance the inverter's thermal balance, and minimise localised heating, thereby extending switch lifetime. Despite being more frequently linked to multilevel converters, PSC offers substantial advantages in terms of decreased switching loss, enhanced device dependability, and overall system efficiency when used in a typical two-level VSI. The method generates a representation of all mathematical function parameters in pseudocode. Figure 2 displays the flowchart for KbMNCF.

4.2. Detailed approach of KbMNCF

Dehghani et al. (2023) [33] presented the Kookaburra Optimisation Algorithm (KOA), a newly created bio-inspired metaheuristic, in the field of biomimetics. The hunting tactics of kookaburras, a species of bird renowned for its cooperative and opportunistic feeding habits, serve as its model. To ensure diversity, KOA functions as a population based search method with two primary phases: exploration, in which agents (candidate solutions) spread widely across the search space to mimic kookaburras searching for prey, and exploitation, in which the agents focus on promising regions, honing their positions to "capture prey" and converge toward optimal solutions. Premature convergence is less likely thanks to KOA's dual technique, which strikes a balance between local refining and global search. KOA is a significant contribution to the field of computational intelligence and optimisation, as it outperforms other nature-inspired algorithms in benchmarking on standard optimisation functions.

4.2.1. Modular network A sophisticated architecture known as a Modular Neural Network (MNN) breaks down a challenging learning task into several specialised modules, each of which is responsible for resolving a different subproblem. To maximise the performance of the KbMNCF, the hyperparameters in the MNN are crucial. PWM

tuning, heat management, voltage control, and torque ripple minimisation are just a few of the specialised responsibilities that each of the architecture's multiple modules handles. The intricacy of the assignment determines the Number of levels each module has. While more complicated functions, such as torque ripple reduction or heat control, may require deeper structures with up to 6–8 layers, simpler tasks may only need 3–4 hidden levels. To accommodate more complex outputs, deeper layers or the output layer may have 128, 256, or even 512 neurons.

On the other hand, initial layers usually have 32 or 64 neurons. Usually set at 0.001, the learning rate is a crucial parameter that can be dynamically adjusted with optimisers such as Adam, which adaptively modify the learning rate during training to achieve faster convergence. To balance training speed and stability, the batch size—which determines the Number of training samples processed before updating the model's weights—is typically set between 32 and 64. Although the Adam optimiser is generally recommended, depending on particular needs, other options such as RMSProp or Stochastic Gradient Descent (SGD) may be employed. Dropout rates, typically set between 0.2 and 0.5 to prevent overfitting and promote generalisation across a range of operating conditions, are also crucial for regularisation. Both hidden and output layers utilise activation functions such as ReLU, sigmoid, tanh, and softmax. ReLReLU is most frequently used for hidden layers due to its effectiveness in training deep networks. To prevent overfitting, the network is typically trained for 50–100 epochs with early termination. Large weights are frequently penalised using L2 regularisation (also known as weight decay) to prevent overfitting from worsening. For tasks such as voltage regulation or PWM signal management, the loss function is typically the mean squared error (MSE). For classification tasks, it is the cross-entropy loss. Data augmentation strategies, such as simulating various load conditions, can be used to artificially enlarge the dataset, while data preparation techniques, like normalisation or scaling, are applied to the input data to ensure consistency and enhance training. The model's generalisability is evaluated by cross-validation or a hold-out validation set. The training data is derived from both simulated environments and real-time operating data from inverter-fed motor systems. To ensure that the network effectively learns to minimise harmonic Distortion, maximise Voltage and efficiency, and provide steady and smooth motor operation under various real-world conditions, all these hyperparameters are adjusted.

4.2.2. PWM tuning by KbMNCF To maximise inverter performance for induction motor drives, the suggested Kookaburra-based Modular Neural Control Framework (KbMNCF) explicitly adjusts crucial PWM settings. The framework modifies the following parameters: the carrier phase shift amount, which distributes switching transitions to lower common-mode voltage and thermal stress on the power switches; the modulation index, which controls the inverter's output voltage magnitude; and the third harmonic injection amplitude, which improves DC bus utilisation and raises the fundamental Voltage. A feedback loop that continuously monitors real-time performance indicators, particularly the torque ripple profile, the predicted system efficiency, and the measured Total Harmonic Distortion (THD) of the output voltage, directs these management operations. By processing this feedback, the KbMNCF adjusts PWM parameters adaptively, balancing switching loss reduction, voltage utilisation, and harmonic suppression. Under various load and operating conditions, the inverter is guaranteed to maintain excellent efficiency and waveform quality due to its closed-loop control technique. Hence, the pseudocode is given in Algorithm 1.

By minimising a multi-objective fitness function, the Kookaburra optimiser is employed in the proposed KbMNCF-based control approach to adjust the control parameters of the PWM process. The fitness function is designed to balance the inverter's key performance metrics, including maximising overall efficiency, decreasing torque ripple, and minimising THD. The Modular Neural Network (MNN), which generates matching PWM gating signals for the Voltage Source Inverter (VSI), first receives a set of candidate PWM parameter values. After simulating or measuring the VSI output, the fitness function is used to assess the performance indices that result. To converge on the ideal PWM parameter set, the Kookaburra optimisation method iteratively updates these candidate solutions based on the direction of the fitness values. By learning the mapping between the optimum PWM settings and input operating circumstances (such as DC voltage and motor load demand), the MNN integrates this process. By ensuring that the MNN weights and control modules are adjusted to minimise the fitness function over a series of iterations, the optimiser effectively integrates optimisation knowledge into the neural architecture. By eliminating the need for repeated optimisation cycles, the MNN can produce optimised PWM gating signals in

Algorithm: KbMNCF

BEGIN
// Step 1: System Initialisation
Initialise DC voltage source
Initialise three-phase VSI
Initialize KbMNCF
Set Kookaburra optimiser parameters (population size, iterations)
// Step 2: Define Fitness Function
Fitness $F = w1 * (1/\text{Efficiency}) + w2 * (\text{THD}) + w3 * (\text{TorqueRipple})$
// Step 3: Generate Candidate Solutions
Create an initial population of candidate PWM parameters.
FOR each candidate solution DO
Feed candidate parameters as input to MNN.
MNN outputs PWM gating signals
Simulate VSI with generated PWM.
Calculate performance metrics: Efficiency, THD, Torque Ripple.
Compute Fitness F for the candidate.
END FOR
// Step 4: Kookaburra Optimisation Loop
WHILE stopping criterion not met DO
Update candidate solutions using Kookaburra search rules.
FOR each candidate DO
Feed to MNN $\rightarrow$ generate PWM $\rightarrow$ simulate VSI
Evaluate Fitness F
END FOR
Store the best candidate with the minimum Fitness.
END WHILE
// Step 5: Update Neural Network
Train/tune MNN weights based on the best candidate's parameters.
Save optimised PWM control rules inside MNN.
// Step 6: Online Operation
FOR each load/voltage condition DO
Provide condition inputs to the trained MNN.
MNN generates optimised PWM parameters directly
Apply PWM to the VSI for motor drive
END FOR
// Step 7: Performance Validation
Assess final performance metrics:
Efficiency $\uparrow$, THD $\downarrow$, Torque Ripple $\downarrow$
Compare against conventional VSI control.
END

real-time after training, ensuring high-quality inverter output with fewer harmonics, smoother torque, and increased energy efficiency.

5. Result and Discussion

To show the effectiveness of the developed model, the charts are compared based on several metrics. This three-phase VSI illustrates the significance of the suggested KbMNCF. A comparison of specific parameters with existing methods demonstrates the efficacy of the concept. Table 1 describes the parameter execution.

Table 1. Execution parameters

Parameter	Description
Platform	MATLAB
Operating System	Windows 10
Version	R2021a
Optimization	Kookaburra
Network	Modular neural network

Device specification

To improve overall performance, reduce harmonic Distortion, and increase system efficiency, SiC MOSFETs and optimised DC-link capacitors are essential components of a high-performance three-phase inverter-fed motor drive that utilises the Kookaburra-based Modular Neural Control Framework (KbMNCF).

Silicon Carbide (SiC) MOSFETs, such as the Cree/Wolfspeed C3M0125090J or Infineon CoolSiCTM MOSFETs (e.g., IPD60R180C7), are the best semiconductor option for such systems. Compared to conventional silicon MOSFETs, these devices offer reduced on-state losses and faster switching speeds, which result in excellent efficiency. They are ideal for demanding industrial applications, as they can withstand higher temperatures and voltages. SiC MOSFETs enable the inverter to operate at higher switching frequencies (50 kHz and above), significantly reducing switching losses and improving overall system efficiency. They have voltage ratings of 900V to 1200V and current ratings of up to 60A. This is essential for maintaining smooth motor functioning and reducing Total Harmonic Distortion (THD).

For high-power inverter systems, usually in the 5–10 kW range, a DC-link capacitor with a voltage rating of 600V–1000V and a value of 470 μF –1000 μF is optimal. Capacitors, such as film or aluminium electrolytic capacitors, are used to stabilise the DC bus voltage and filter out switching noise. The low ESR properties of these capacitors are crucial for reducing ripple currents, which can cause thermal stress and power losses. To ensure dependable functioning under a range of load situations, the capacitor's voltage rating must be at least 1.5 times higher than the peak DC voltage.

5.1. Case study

The MATLAB model utilised for the three-phase VSI is provided in this case study. This inverter converts a DC input into a balanced AC output, as proposed in the KbMNCF. The three-phase inverter is incorporated with the PWM generator. The Kookaburra fitness function was embedded in the suggested method.

This simulation diagram illustrates an entire MATLAB/Simulink model of a three-phase inverter controlling an induction motor (IM) with harmonic analysis. The left part includes the three-phase inverter interfaced with a PWM generator, which modulates IGBT switching based on modulating signals. The inverter is supplying a 3 HP, 220V, 50 Hz, 1500 rpm induction motor (IM), which is mechanically loaded. Sensors monitor key parameters, including speed, torque, and electrical signals. The top right part indicates speed measurement and reference speed comparison. The calculation of the THD of current and Voltage is done with the help of harmonic analysers, which are represented in the middle part of the diagram. The bottom part appears to be two-level inverter blocks or harmonic filter subsystems for more specific signal processing or enhancement. In general, the simulation is designed to evaluate motor performance and harmonic Distortion in the system under PWM control.

The rotor speed response of a three-phase inverter-fed IM over a short period is displayed in Figure 3. The x-axis shows time, while the y-axis shows the rotor speed in radians per second. Initially, the speed rapidly decreases, indicating a slowdown that can be induced by a change in torque or a load disturbance. Following this, there is a

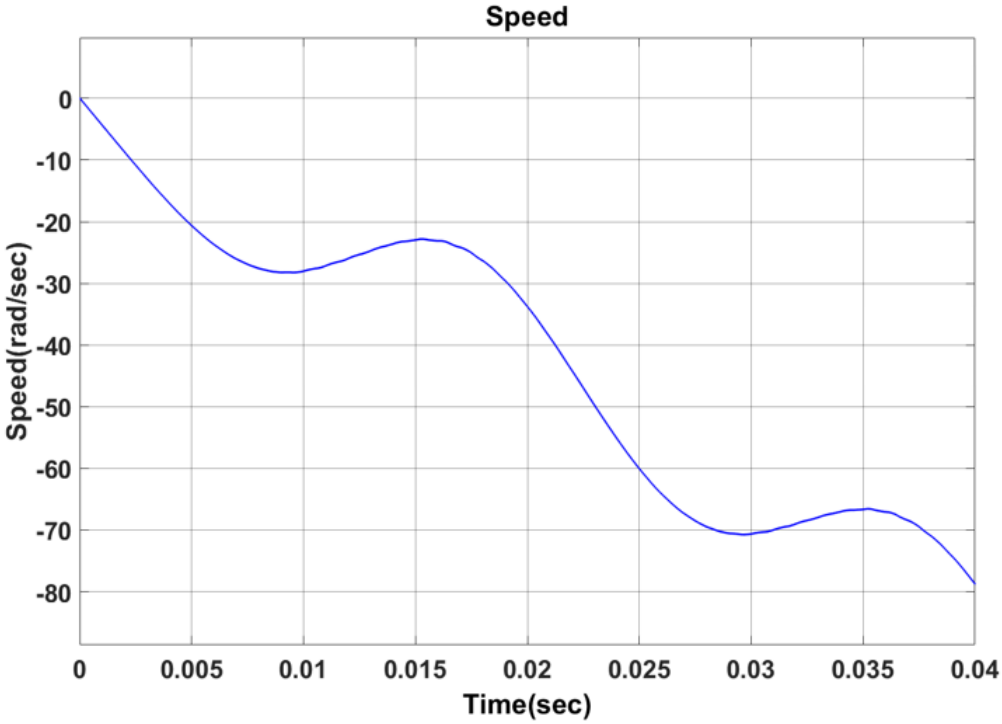

Figure 3. Three-phase inverter-fed IM rotor speed

brief bounce before another loss, exhibiting dynamic oscillating behaviour. As the system attempts to settle under varying electromagnetic torque and load conditions, the curve illustrates the motor's fluctuating behaviour under the influence of the edge-shifted carrier modulation and trapezoidal reference.

Figure 4 shows the electromagnetic torque generated by the inverter-fed induction motor (IM) over the same period. The torque increases in a pulsating pattern, peaking in the middle of the interval before decreasing and then increasing again, creating a waveform featuring periodic ripples. These ripples are characteristic of PWM-controlled drives and are affected by the switching behaviour of the inverter. The graph highlights the dynamic character of the torque and its analogy with the observed speed oscillations in Figure 4.

The three-phase inverter-fed IM's stator current waveform is shown in Figure 5. The x-axis and y-axis indicate time and current, respectively, in amperes. As is typical of PWM inverter outputs, the waveform displays a roughly sinusoidal pattern with discernible ripple components. Indicating balanced current flow in the stator windings, the current rises and falls symmetrically, showing two major peaks within the measured time range. The inverter's switching activity produces ripples that are overlaid on the waveform, and the modulation method, in this instance, a trapezoid reference with edge-shifted carriers, is reflected in the magnitude of the ripples.

There are two subplots in Figure 6. The phase voltages of the inverter output are displayed in the top subplot, where three different colour-coded signals represent the three phases. These voltage signals, which are indicative of space vectors or advanced PWM methods, appear as high-frequency PWM waveforms that alternate between positive and negative peaks. The matching phase currents, which are flatter waveforms approaching sinusoids for each phase, are displayed in the bottom subplot. The motor's reaction to the PWM voltage inputs is evident in these current waveforms, which maintain a balanced three-phase profile. When combined, these figures show how the IM drive system efficiently generates and regulates three-phase voltages and the ensuing phase currents.

The inverter's output voltage waveform is displayed in Figure 7. By combining the edge-shifted PWM signal with the sinusoidal reference, a stepped waveform is created that simulates a sine wave. The waveform demonstrates

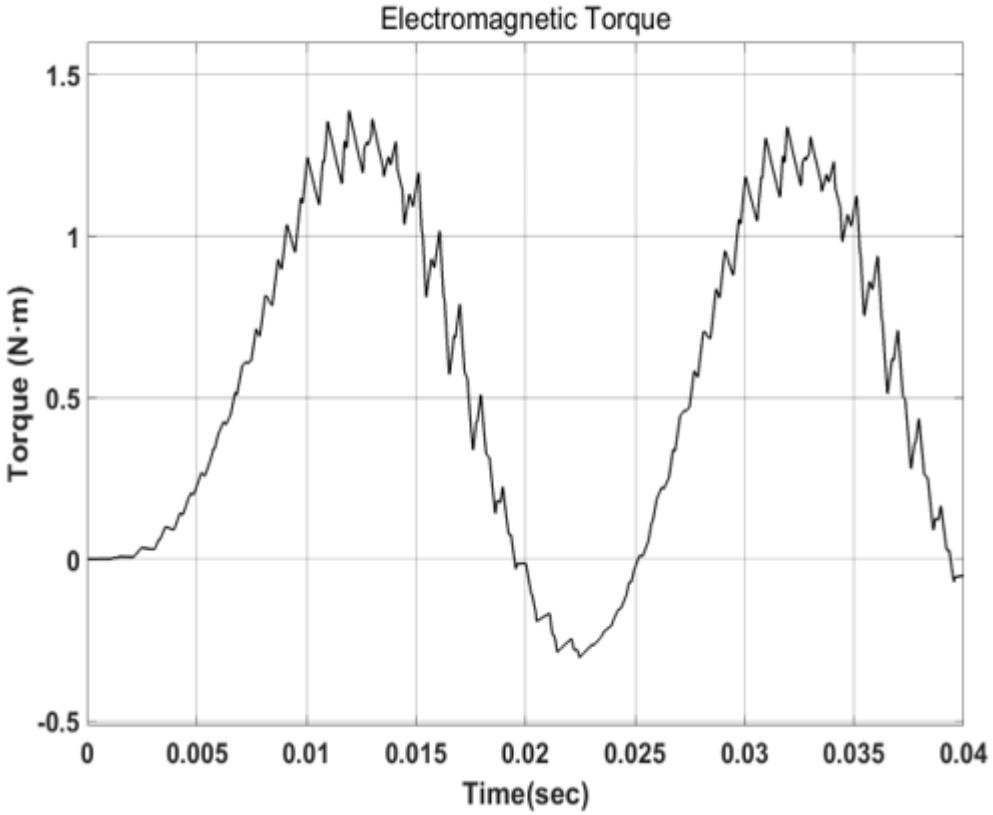

Figure 4. Electromagnetic torque

how well the inverter produces a nearly sinusoidal output, assisting in providing the IM with steady and effective power.

The inverter is regulated by PWM switching pulses, as shown in Figure 8. By comparing the edge-shifted carrier signals with the modulated reference signal, these high-frequency pulses are generated. The output voltage can follow the appropriate waveform since the rapid ON and OFF pulses switch the inverter's power devices. This method lowers harmonic Distortion and enhances voltage control in the motor drive system.

Figure 9 illustrates the frequency content of the output signal of a third harmonic injected and edge-shifted PWM carrier three-phase inverter driving an IM. THI improves voltage utilisation and minimises Distortion, and edge shifting disperses the harmonic frequencies into lower electrical noise. The small spikes in the graph indicate harmonic frequencies, and their low amplitude suggests that the unwanted harmonics are being reduced, allowing the motor to receive a cleaner, more efficient signal.

Figure 10 indicates the three subplots of PWM modulation and signal analysis. The modulating waveform used to create PWM signals is displayed in the top subplot; it is most likely a sine wave that has been altered using harmonic injection. PWM is produced by the carrier signal or switching pulses interacting with the modulating signal, as seen in the middle subplot. The resulting duty cycle or amplitude fluctuation, which illustrates how the PWM pulse widths change in response to the modulating signal, is shown in the bottom subplot.

There are two plots in Figure 11. The top plot displays the three-phase output voltages of the inverter following PWM switching. Before filtering, the Voltage appears as fast-switching square-like waveforms, which are typical of an inverter output. The matching three-phase current waveforms of the IM are shown in the bottom plot. These are 120° phase-shifted and sinusoidal, demonstrating how well the motor filters the PWM and generates steady currents.

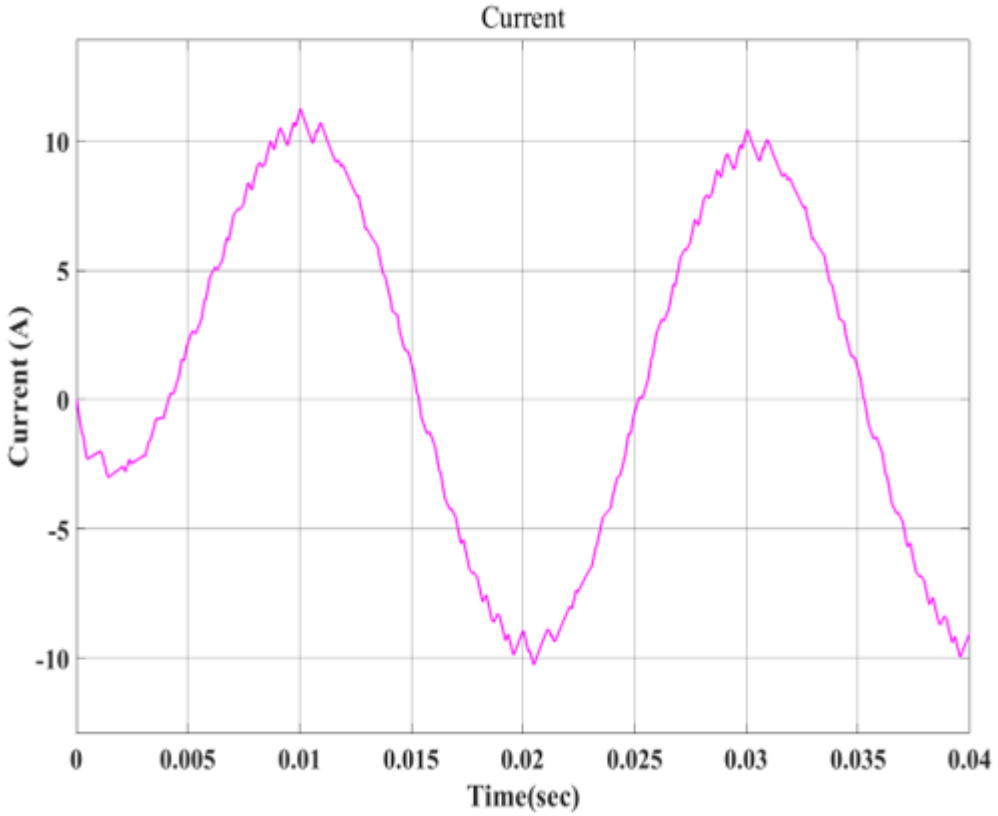

Figure 5. The three-phase inverter-fed IM's stator current waveform

A high-frequency PWM waveform with sinusoidal envelopes, characteristic of sinusoidal PWM (SPWM), is displayed in Figure 12. A sinusoidal pattern is observed in the average over time, despite the waveform's rapid transitions between positive and negative values. This indicates that a triangle carrier wave is modulated using a sinusoidal reference, resulting in the output voltage.

In Figure 13, the THI in the PWM approach is illustrated in a three-phase inverter. The red wave represents the high-frequency triangular carrier wave, while the blue wave represents a fundamental sine wave with the third harmonic component added. The resulting modulation of the green and pink lines indicates reference signals of different phases. The top of the reference waveform is smoothed by adding the third harmonic, which allows a higher modulation index without exceeding carrier limits. Improved output waveform quality and reduced voltage usage result in lower Total Harmonic Distortion (THD) and enhanced inverter performance.

The actual gate pulses produced by the PWM controller for a single inverter switch are probably displayed in Figure 14. These binary signals directly control the power electronic switches. The inverter's AC output is based on the pulse width variation, which represents the PWM action to follow the intended sine wave envelope.

Figure 15 illustrates how, in PWM for a three-phase inverter, THI alters the sinusoidal reference to remain inside the high-frequency triangle carrier. It improves voltage usage and lowers THD by flattening the peaks, allowing an improved modulation index without over-modulation.

Figure 16 illustrates the reference signals with THI, which are used to create PWM pulses for a three-phase inverter, including THI. The three sinusoidal traces are transformed by the inclusion of a third harmonic component, which slightly reduces the peak voltages and improves voltage utilisation. The waveforms are uniformly spaced 120 degrees apart and assist the inverter in creating an efficient and balanced output for the IM. The inclusion of the TH enables the inverter to develop a higher output voltage without exceeding the DC bus limit, thereby enhancing motor performance.

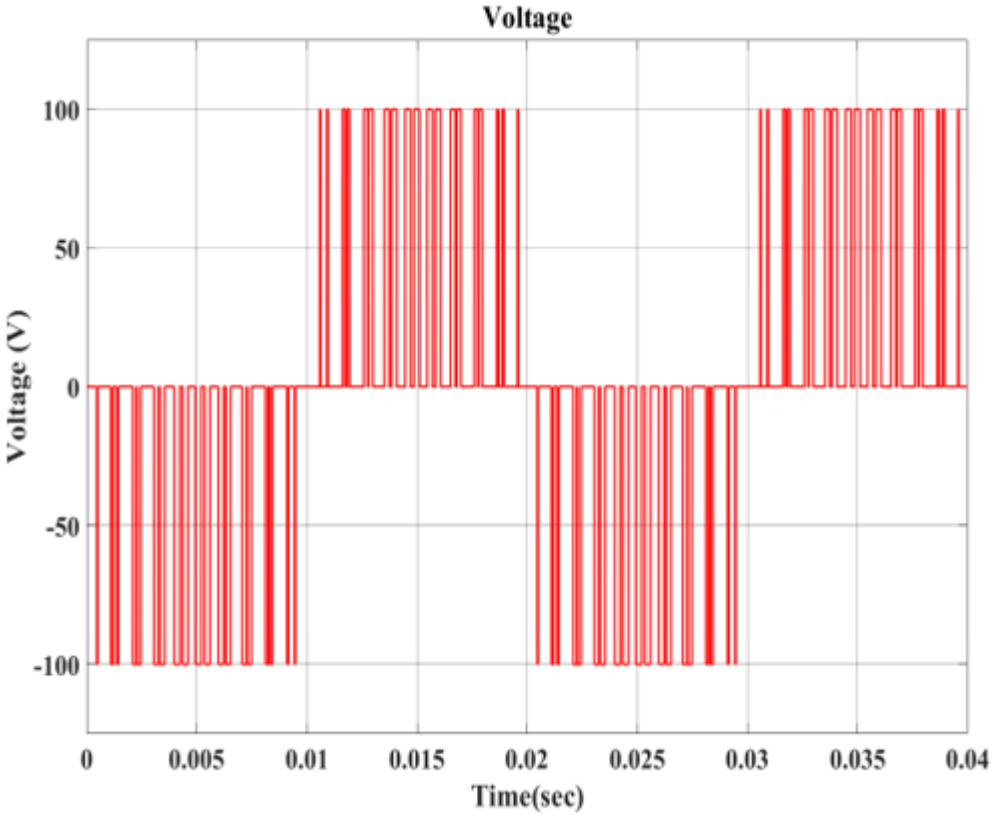

Figure 6. The two subplots of inverter output phase voltages and matching phase currents

THI is used to generate PWM signals, as shown in Figure 17. The triangle carrier signal is displayed at the top, followed by the reference waveform in the middle, and the final PWM output at the bottom. By comparing the reference with the carrier, the PWM signal is generated, providing the inverter with accurate switching pulses. This technique is ideal for applications involving efficient motor drives, as it enhances voltage utilisation and helps reduce Total Harmonic Distortion (THD).

Figure 18 illustrates three reference waveforms of modulation for a three-phase THI inverter. The red, blue, and yellow lines represent the reference signals for the three phases, respectively, each shifted by 120°. The introduced third harmonic causes the waveforms to appear ”flattened” at the peaks compared to pure sine waves, allowing for more voltage utilisation without exceeding the carrier limit in PWM. This technique enhances the inverter’s output performance while reducing Total Harmonic Distortion (THD).

Figure 19 shows the variance between a carrier signal and a tuned reference waveform, as well as the resultant output of a PWM or line voltage waveform. The blue waveform displays a higher-frequency triangle carrier used for pulse width modulation (PWM), whereas the red waveform depicts a reference signal with harmonic components. The combination of the modulating and carrier signals changes the yellow waveform, which appears to be the created output or line voltage following PWM switching. This demonstrates how a basic DC input can be used to create complex waveforms through pulse-width modulation (PWM).

Three-phase-shifted PWM reference waveforms, which frequently appear in three-phase inverter systems, are displayed in Figure 20. The curves represent the regulating signals for the three phases. These signals are sinusoidal with additional harmonics. To create a balanced three-phase output, these signals are shifted by 120 degrees relative to each other. The waveform shapes indicate that harmonic injection is employed to enhance motor drive efficiency and inverter performance by increasing voltage utilisation and reducing Total Harmonic Distortion (THD).

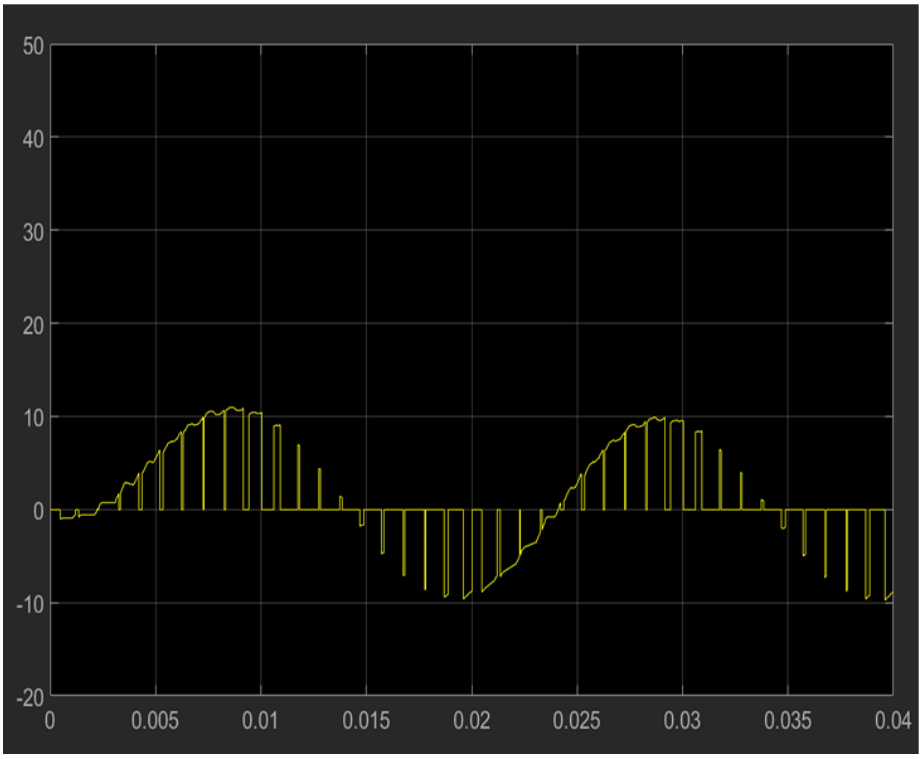

Figure 7. Inverter Output Voltage Waveform

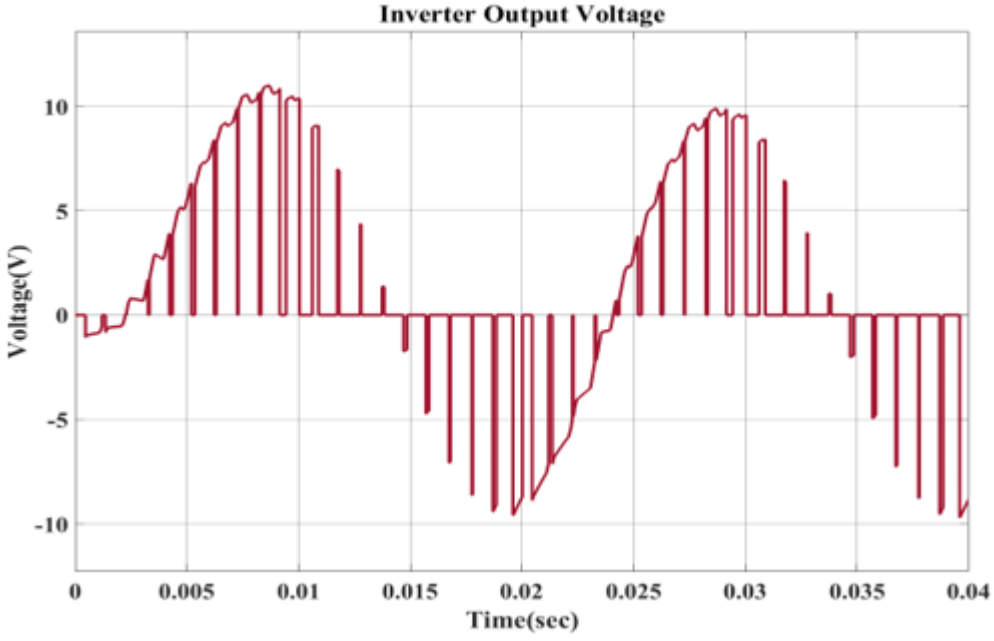

Figure 8. PWM Switching Pulses

A three-phase inverter with THIPWM is illustrated in Figure 21 through three modulating waveforms. These waveforms represent three 120-degree-apart reference signals of the three phases. These signals contain a third

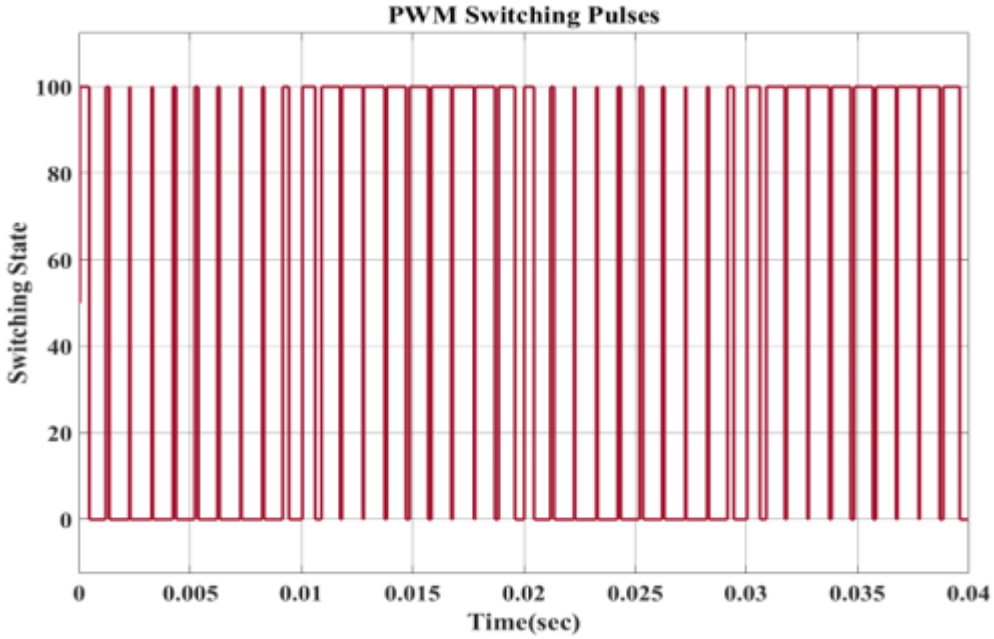

Figure 9. Output signal of THI

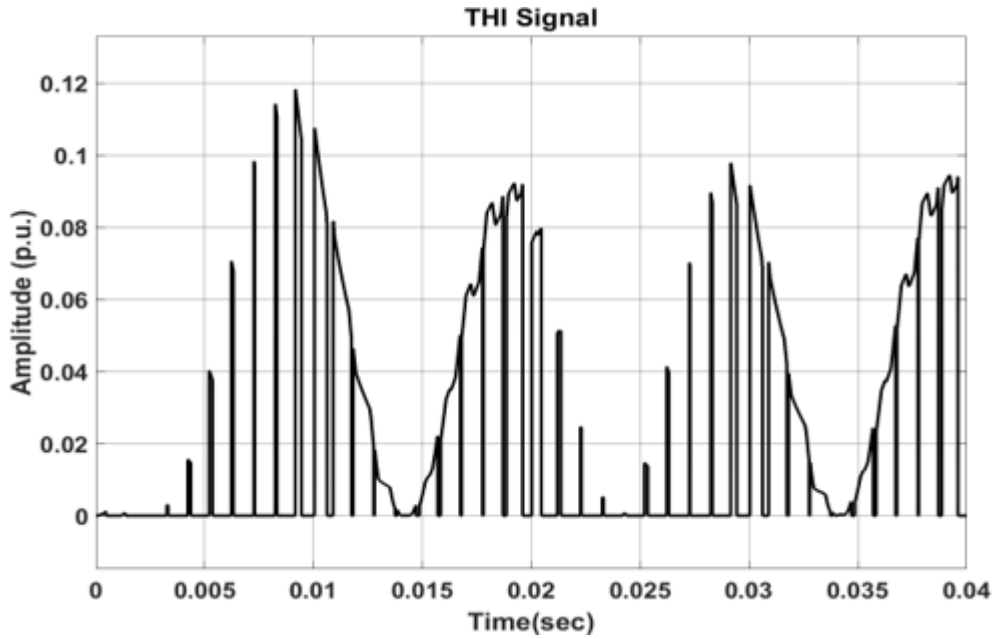

Figure 10. Three Subplots - PWM Modulation & Signal Analysis

harmonic component, which narrows the zero crossings and reduces the peaks slightly compared to pure sine waves. Without increasing the DC input, this technique raises output voltage utilisation to approximately 87% of the DC bus. By cancelling the line-to-line voltages, the third harmonic, identical in all three phases, maintains a sinusoidal output, reduces total harmonic Distortion (THD), and improves inverter efficiency.

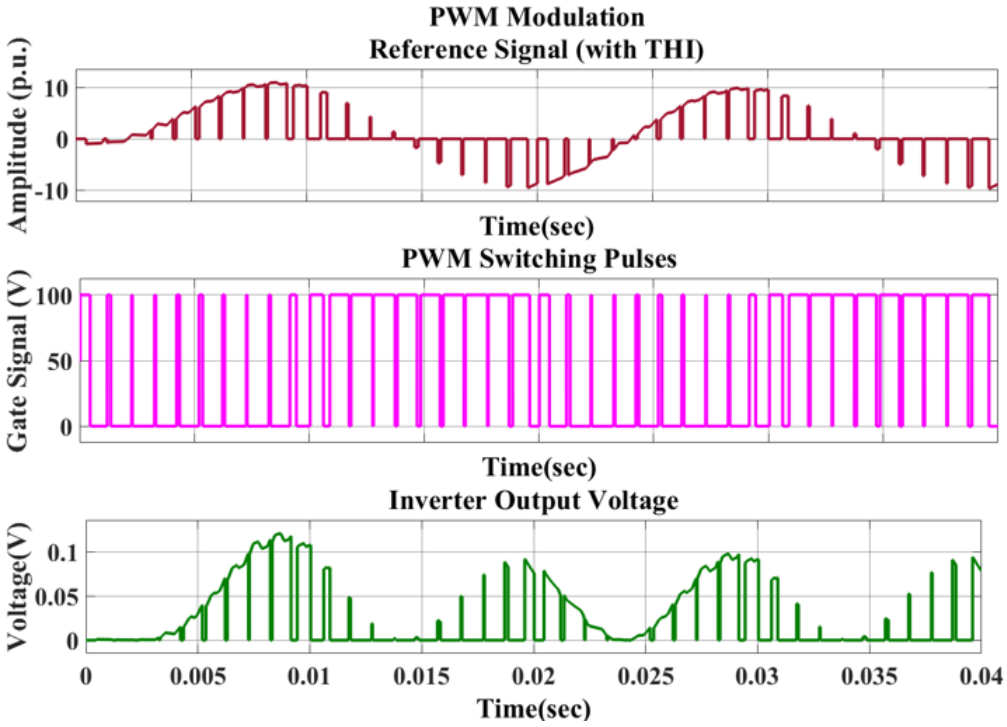

Figure 11. Inverter Output Voltage and Motor Currents

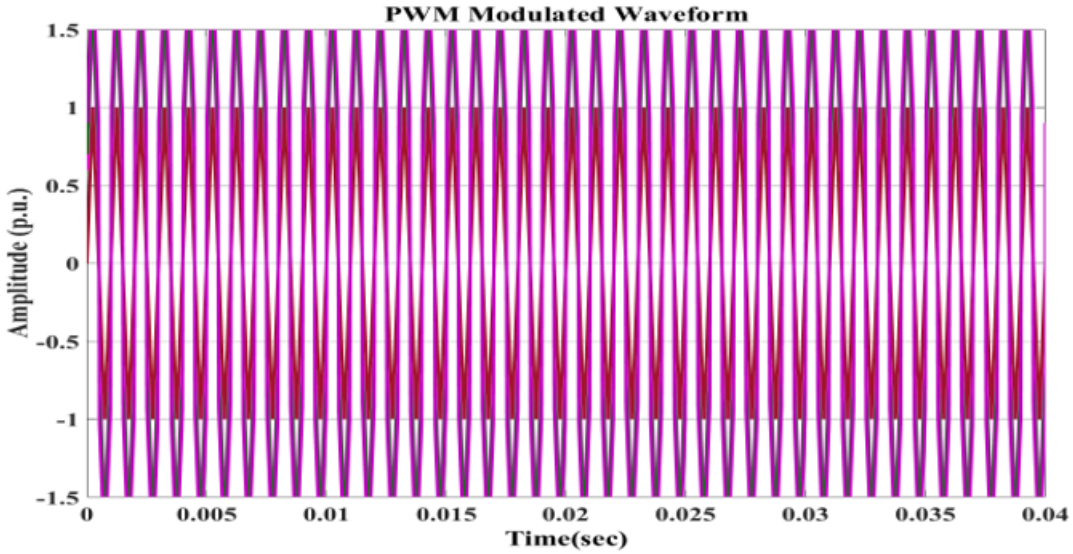

Figure 12. PWM Modulated Waveform

Figure 22 shows the sinusoidal waveform. This waveform is a sinusoidal waveform with its shape slightly adjusted, and it is most likely a reference signal with THI applied to a three-phase inverter for an IM. The fundamental sine wave is combined with a third harmonic to enhance voltage utilisation. This method reduces

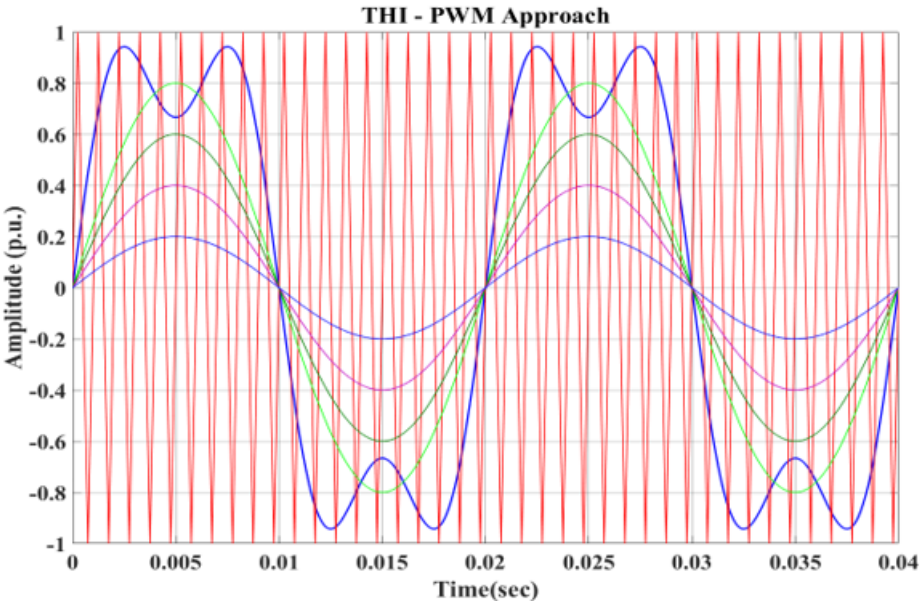

Figure 13. THI in PWM approach

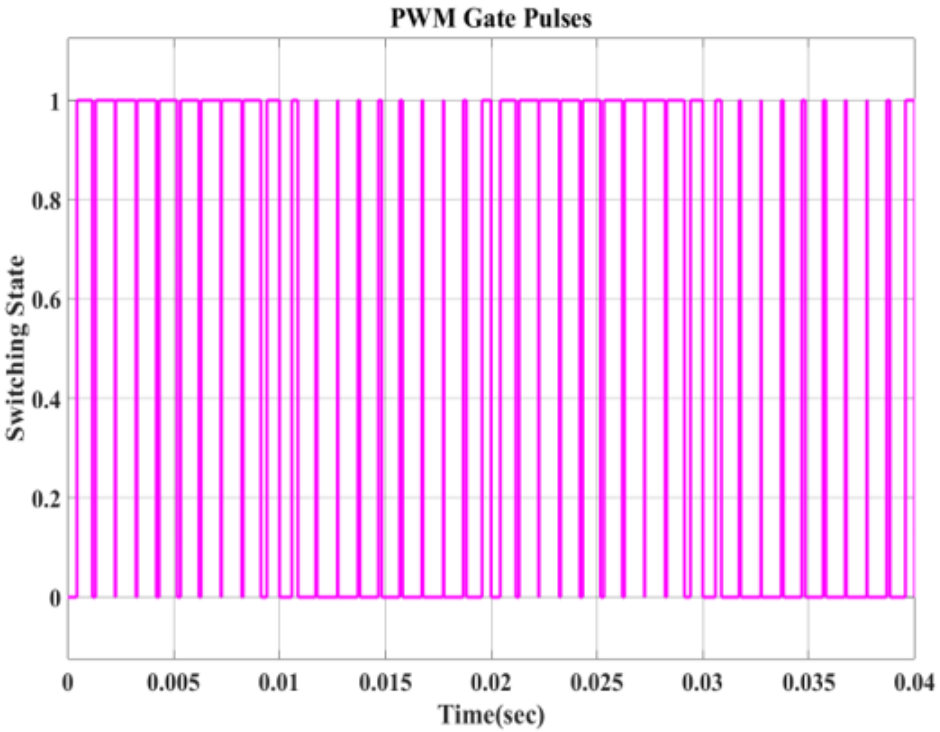

Figure 14. PWM Gate Pulses

power loss and more efficiently utilises the DC supply. The smooth curve indicates that the reference signal has been pre-calibrated before using edge shifted PWM, which helps produce a cleaner and more efficient motor output.

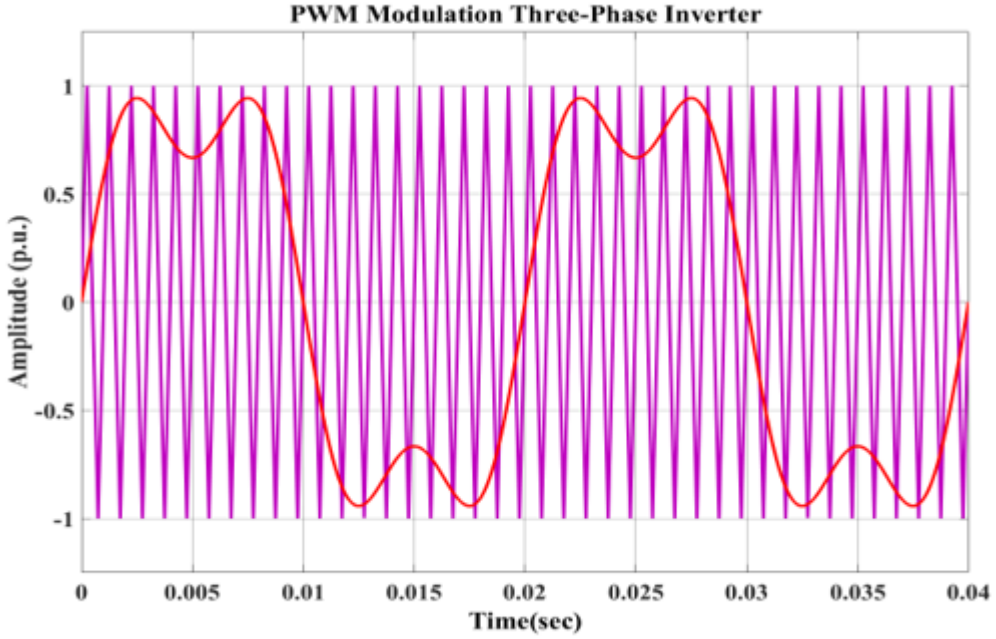

Figure 15. Effect of THI on PWM Modulation in Three-Phase Inverter

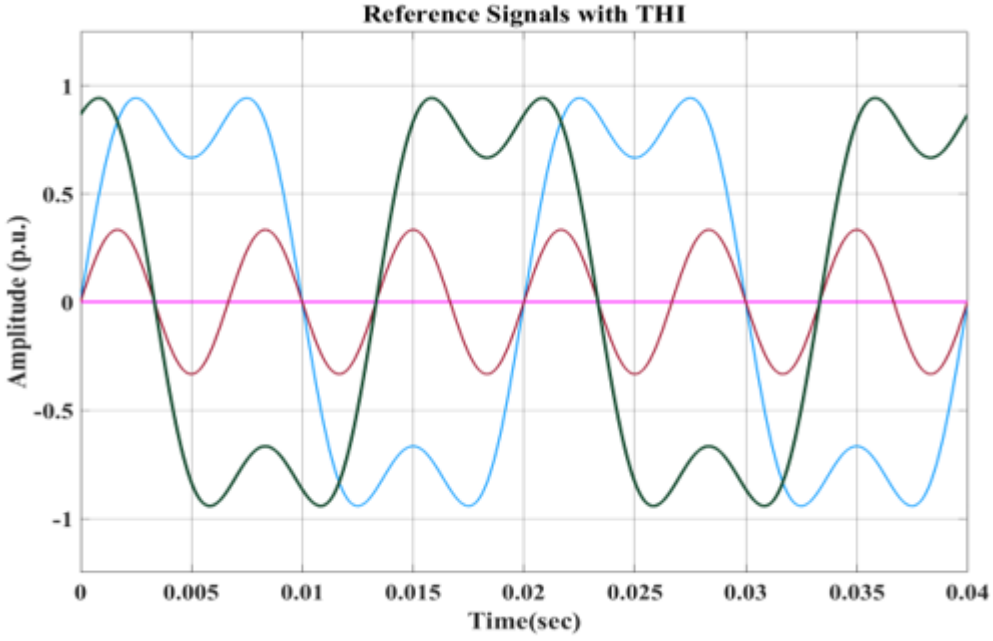

Figure 16. Reference Signals with THI

Figure 23 illustrates a sequence of modulating waveforms with increasing third harmonic content, or modulation index, commonly used in PWM approaches, such as THIPWM. With an increase in the harmonic level, the waveforms get flatter at the peaks and steeper at zero crossings, facilitating improved utilisation of the DC bus

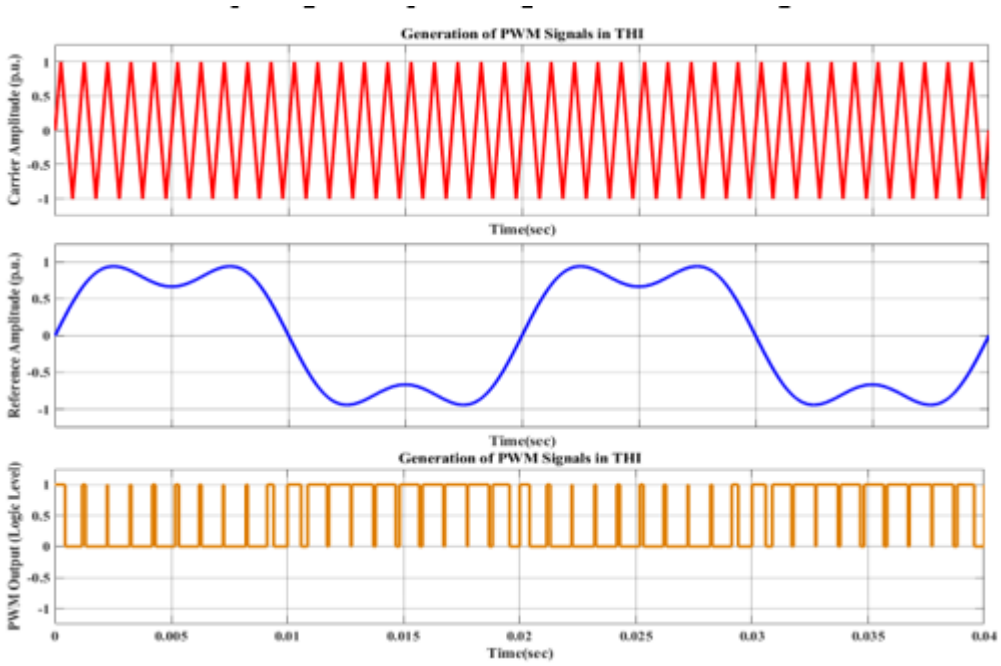

Figure 17. Generation of PWM signals in THI

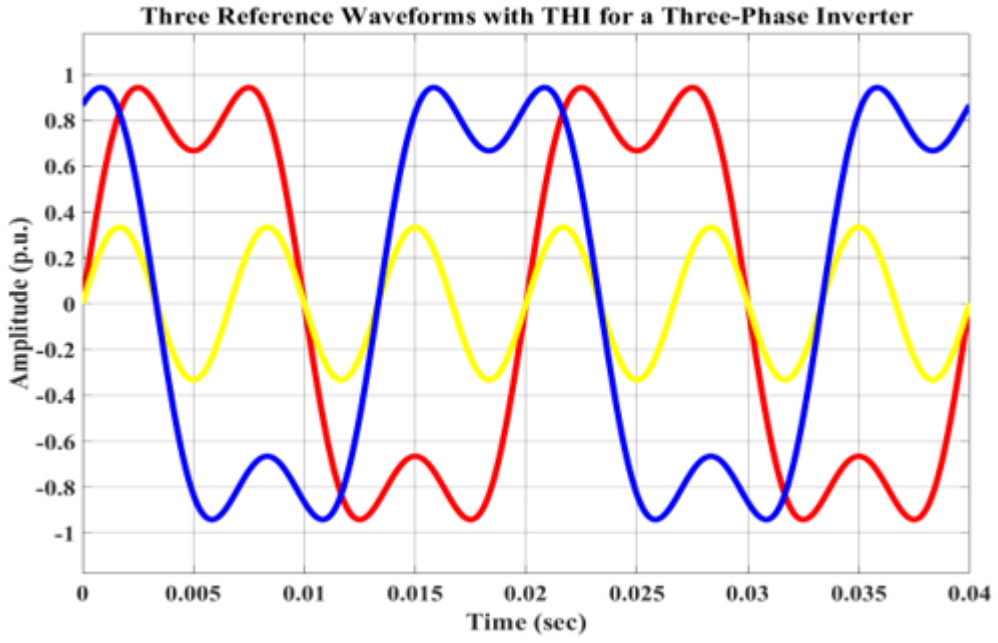

Figure 18. Three reference waveforms of modulation for a three-phase THI inverter

voltage and enhanced inverter performance. The method facilitates improvement in the output voltage without distorting line-to-line voltages and minimises total harmonic Distortion (THD).

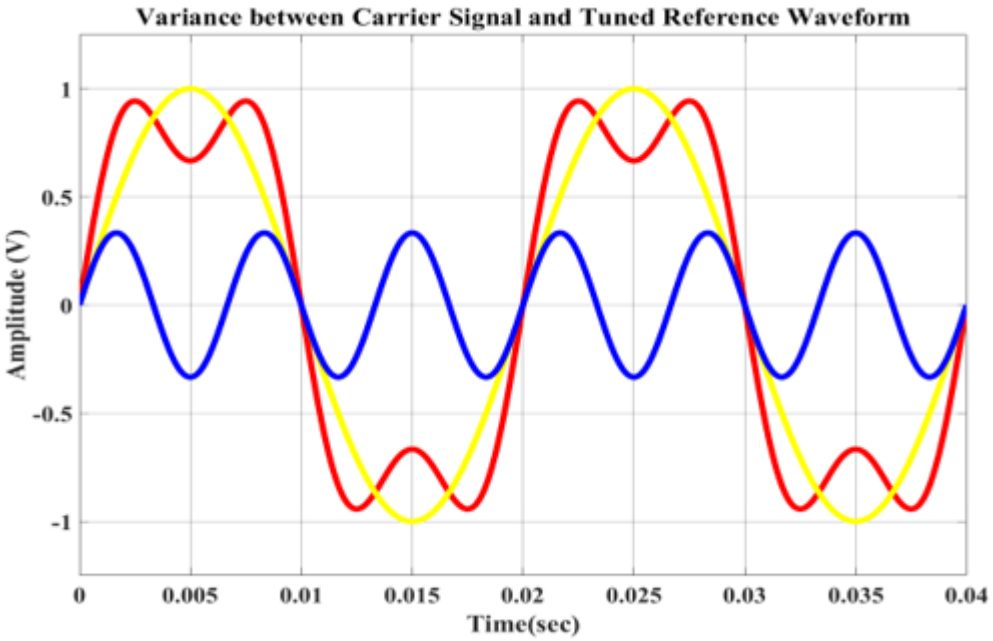

Figure 19. Variance between a carrier signal and a tuned reference waveform

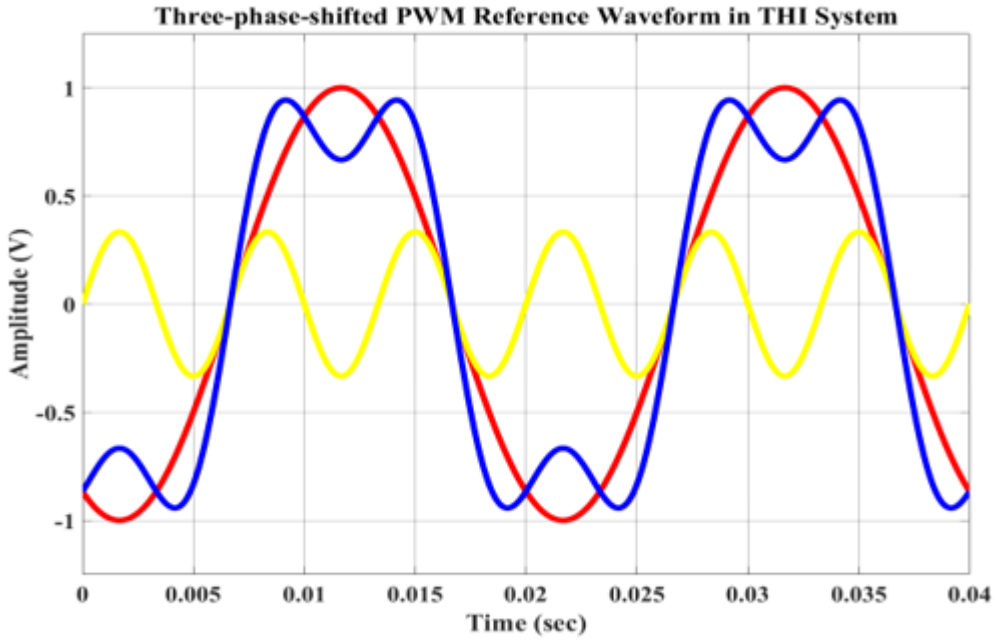

Figure 20. Three-phase-shifted PWM reference waveforms in THI systems

The major components of the signal, especially the fundamental frequency (50 Hz) and its harmonics (100 Hz, 150 Hz, etc.), are represented by the relatively high peaks at the lower frequencies at the beginning of the figure. The amplitude, however, drastically drops as we move from left to right on the x-axis (up to 5 kHz), suggesting that the higher frequency harmonics contribute far less energy to the signal. Most signals exhibit this slow decline, with

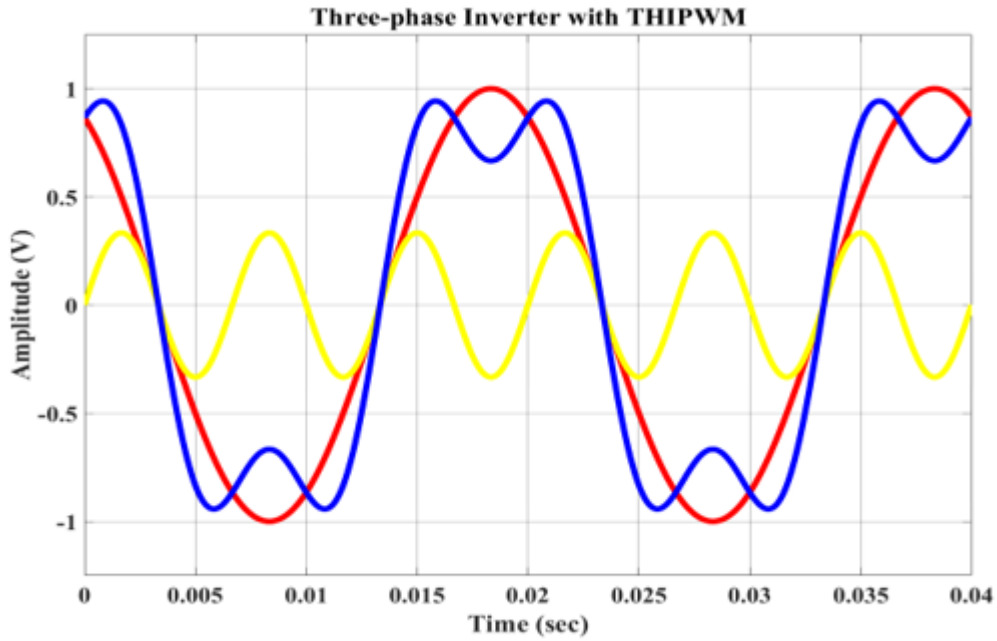

Figure 21. Three-phase inverter with THIPWM

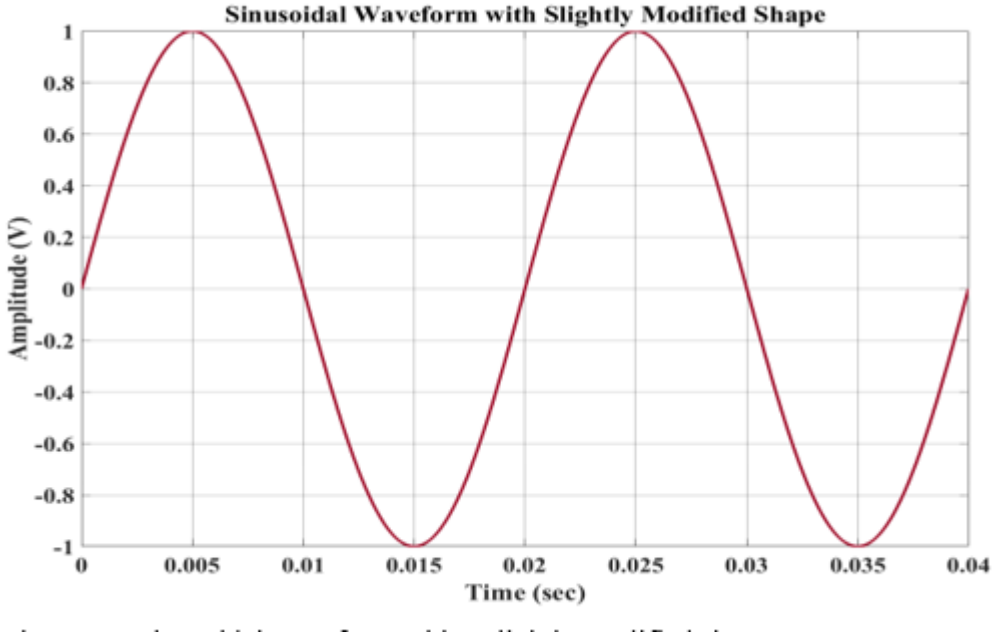

Figure 22. Sinusoidal waveform with a slightly modified shape

stronger harmonics comprising a smaller portion of the overall waveform, particularly in motor-driven systems or inverter outputs.

As is common in many real-world systems, the signal appears to be dominated by lower-frequency components, as indicated by the abrupt reduction in amplitude that occurs after the fundamental frequency and its harmonics.

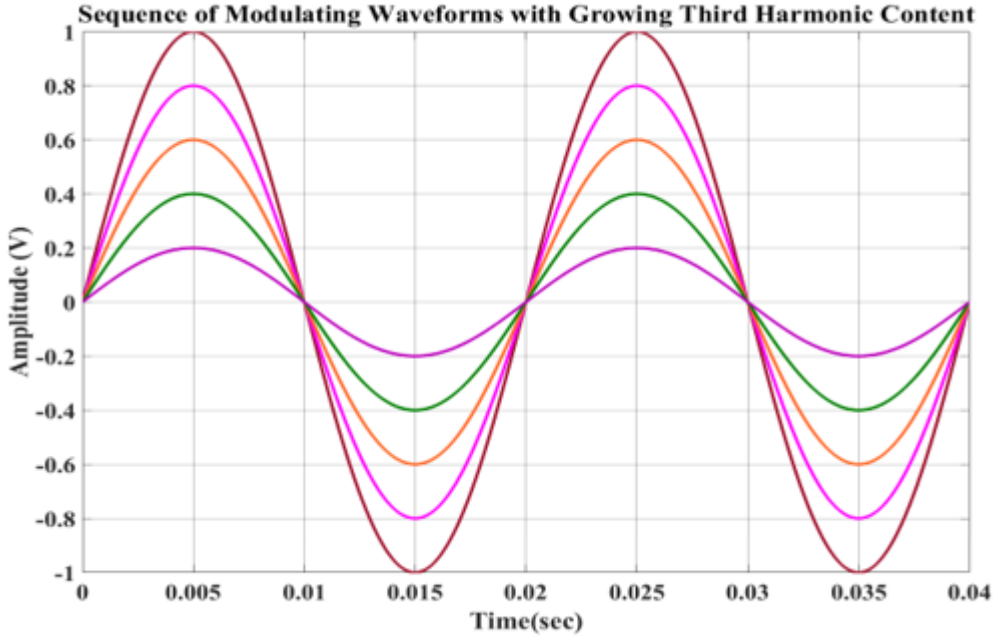

Figure 23. Sequence of modulating waveforms with growing third harmonic content or modulation index

The steep decay indicates that higher-frequency harmonics are damped, a typical effect when employing methods like PWM to drive motors. Meanwhile, the strong initial amplitude reveals the strength of the fundamental and some lower-order harmonics.

Table 2. MI and THD validation

Modulation Index (MI)	Total Harmonic Distortion (THD) (%)
0.2	16.5
0.4	12.8
0.6	8.7
0.8	4.5
1.0	2.4

THD is compared at different modulation indices (MIs), which range from 0.2 to 1.0, as shown in the table. In PWM schemes, the modulation index regulates the output waveform's amplitude in relation to the carrier signal. The output signal approaches a pure sinusoidal waveform as the modulation index increases, thereby reducing the system's harmonic Distortion. The output waveform is severely distorted at lower modulation indices, such as 0.2 or 0.4, resulting in higher THD values of 16.5% and 12.8%, respectively. This indicates that there are more harmonic frequencies in the signal than fundamental frequencies, which can reduce system performance and lead to problems such as EMI and motor heating. The THD dramatically drops to 4.5% and 2.4%, respectively, as the modulation index rises near 0.8 and 1.0. The output signal is quite near a perfect sine wave when the modulation index reaches its lowest THD of 1.0. The trade-off between harmonic Distortion and the system's capacity to deliver an effective, high quality output voltage is highlighted by the link between the modulation index and THD.

5.2. Performance analysis

The validation of metrics such as Voltage, system efficiency, and THD assesses the effectiveness of the developed model. It is compared with a few existing approaches, including Space Vector PWM (SVPWM), Virtual SVPWM (VSVPWM), Sinusoidal PWM (SPWM), hybrid PWM (HPWM) [31], Level Shift- PWM (LS-PWM), and Reduced CMV SPWM (RCMV-SPWM) [32] that ensure a performance improvement.

5.2.1. THD The amount of Distortion in a signal caused by harmonic components is measured by THD. It shows the degree to which the waveform departs from an ideal sinusoid. It is formulated in Eqn. (8).

$$\text{THD} = \frac{\sqrt{V_2^2 + V_3^2 + \ldots + V_{50}^2}}{V_1} \times 100\% \tag{8}$$

Here, V_1 indicates the RMS value of the fundamental frequency component; the RMS values of the harmonic components are given by $V_2 + V_3 \ldots V_{50}$.

Here V_2 to V_{50} are the second and 50^{th} harmonic components' respective RMS values. A band-limited Fast Fourier Transform (FFT) with a bandwidth up to the 50th harmonic (usually 2.5 kHz for 50 Hz systems) is used to measure the harmonic content. Before sampling, high-frequency noise above the Nyquist frequency is suppressed using an anti-aliasing low-pass filter. During FFT analysis, appropriate windowing (such as the Hanning window) is employed to reduce spectral leakage and enhance measurement accuracy. In accordance with IEEE 519 rules, all measurements are made at the Point of Common Coupling (PCC), which supports a real-world power system.

Table 3. Performance of THD

Methods	**THD (%)**
SVPWM	76.99
VSVPPWM	79.90
Proposed	2.4

The SVPWM achieved 76.99%, the VSVPPWM achieved 79.90%. The THD of the proposed KbMNCF method for the compared mechanism was 2.4% at a modulation index of 0.8, as shown in Table 3.

5.2.2. Voltage The efficiency with which an inverter or power electronic converter generates an AC output voltage from the available DC voltage is measured by its voltage conversion efficiency. It represents the proportion between the DC bus voltage and the highest feasible output AC voltage. It is formulated in Eqn. (9).

$$Voltage = \left(\frac{V_{ph,rms}}{V_{dc}/\sqrt{3}}\right) * 100\% \tag{9}$$

Here, $V_{ph,rms}$ indicates the voltage output phase's RMS value and V_{dc} is the DC input voltage.

The findings of the voltage evaluation are presented in Figure 24. The comparison between the accuracy of the developed model and other well-known methods demonstrates its superior performance. The proposed model produced a 47.833% voltage for KbMNCF. The voltage utilisation of LS-PWM RCMV-SPWM was 42% and 16%, respectively.

5.2.3. System Efficiency The measure of system efficiency is the proportion of input power that is effectively transformed into usable output power. It is formulated in Eqn. (10).

$$SystemEfficiency = \left(\frac{P_{out}}{P_{in}}\right) \times 100\% \tag{10}$$

Here P_{out} P_{in} are the input and output power.

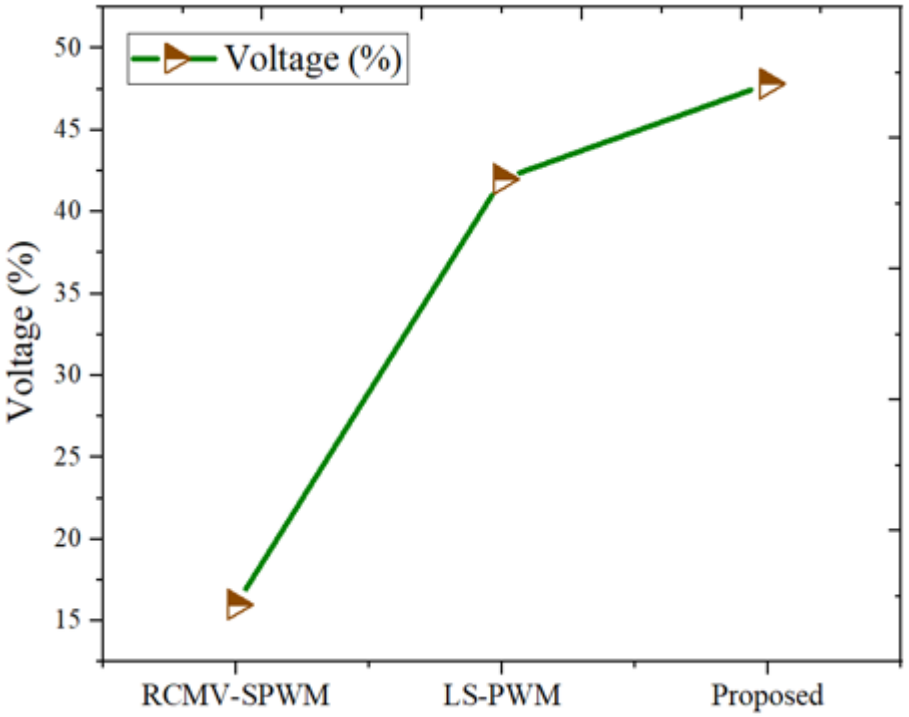

Figure 24. Comparison of Voltage

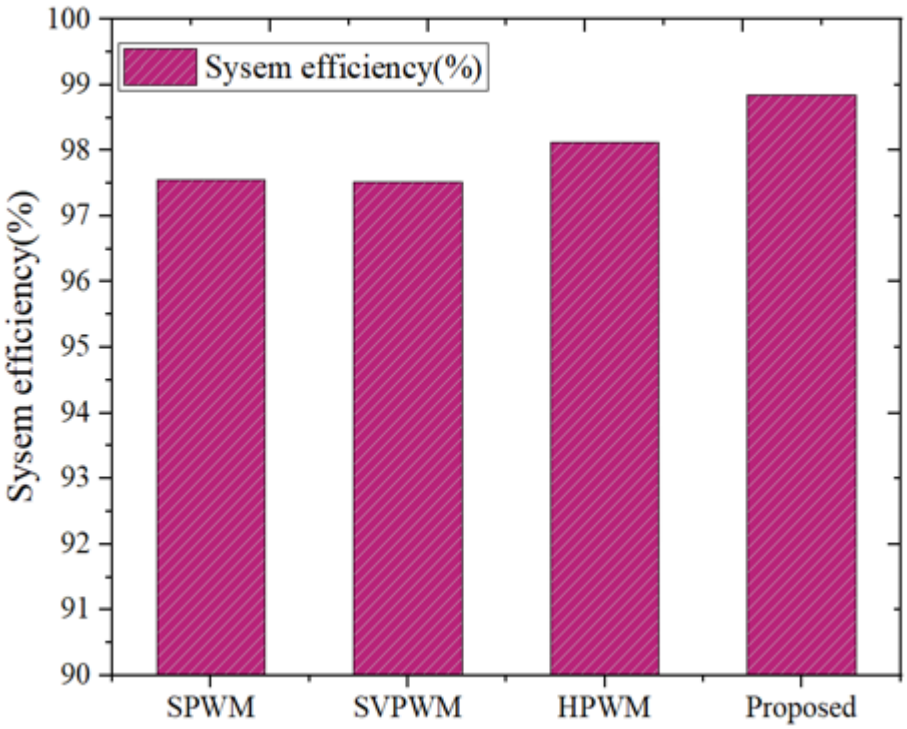

Figure 25. Comparison of System Efficiency

Figure 25 indicates the system efficiency assessment. The proposed method has an efficiency of 99%, and the efficiencies of SPWM, SVPWM, and HPWM are 97.55%, 97.52%, and 98.13%, respectively. The suggested model's high efficiency proved its efficacy.

5.3. Discussion

The developed model's primary objective was to examine a three-phase voltage source inverter (VSI) using advanced pulse-width modulation (PWM) methods. A comparison analysis was included in the last phase of the study to confirm the increase in efficiency. The Kookaburra optimisation methodology was employed in the proposed strategy to overcome the limitations. To effectively drive an IM, the current study helps convert a DC input into a balanced three-phase AC output.

Here, all the compared models, such as Model Predictive Control (MPC), Long Short-Term Memory-based PWM (LSTM-PWM), Deep Reinforcement Learning PWM (DRL-PWM), Generative Adversarial Network PWM (GAN-PWM), Radial Basis Function PWM (RBF-PWM) and Convolutional Neural Network-based PWM (CNN-PWM), were executed in the same proposed platform and outcomes were compared with each other in Table 4. In that, the proposed has the lowest Total Harmonic Distortion (THD) at 2.4%, suggesting excellent waveform quality. With a voltage consumption of 49.0%, the Proposed System (KbMNCF) outperforms the other approaches and exhibits optimal voltage utilisation.

With an impressive efficiency of 99.0%, the Proposed System (KbMNCF) surpasses all other approaches when assessing system efficiency. With the lowest Torque Ripple percentage of 4.5% among the studied methods, the KbMNCF system exhibits smoother motor running and fewer variations in torque delivery. Last but not least, the Proposed System (KbMNCF) achieves the maximum Common-Mode Voltage (CMV) Reduction at 45.5%, significantly lowering bearing currents and electromagnetic interference (EMI), enhancing the motor's dependability and lifespan. This thorough comparison demonstrates the superior performance of the KbMNCF system in terms of torque smoothness, efficiency, voltage usage, harmonic Distortion, and CMV reduction.

Table 4. Benchmark validation with different metrics

Metric	Proposed System	MPC-PWM	DRL-PWM	CNN-PWM	LSTM-PWM	GAN-PWM	RBF-PWM
Total Harmonic Distortion (THD) (%)	2.4%	3.0%	2.6%	2.8%	2.7%	2.9%	2.8%
Voltage (%)	49.0%	45.5%	46.5%	46.3%	46.0%	46.1%	46.2%
System Efficiency (%)	99.0%	97.5%	98.2%	98.1%	97.9%	98.0%	98.3%
Torque Ripple (%)	4.5%	5.0%	5.2%	5.1%	5.3%	5.4%	5.2%
Common-Mode Voltage (CMV) Reduction (%)	45.5%	42.0%	43.0%	42.5%	43.2%	43.1%	42.8%

Overall, the Proposed System (KbMNCF) outperforms both Model Predictive Control and cutting-edge AI-driven PWM techniques by at least 3%, demonstrating significant improvements in THD, Voltage, and System Efficiency. This makes it a more dependable and efficient solution for high-performance inverter-fed motor drives.

By contrasting its performance with alternative methods, the outstanding outcomes of the proposed model are illustrated. The outcomes of the suggested approach are evaluated using the following metrics: total harmonic Distortion (THD), system efficiency, and Voltage. When compared to the available data, the suggested method yields good results.

Over one cycle, the Figure 26 a) compares the ideal inverter output waveform to the non-ideal switching situation. The perfect waveform is smooth and sinusoidal, while the non-ideal waveform has flat areas and minor ripples. Dead-time, switch rise/fall times, and parasitic effects add delay and Distortion to transitions.

The harmonic spectrum graph contrasts ideal and non-ideal switching inverter output frequency-domain characteristics. For high waveform purity, the spectrum should be dominated by the fundamental frequency

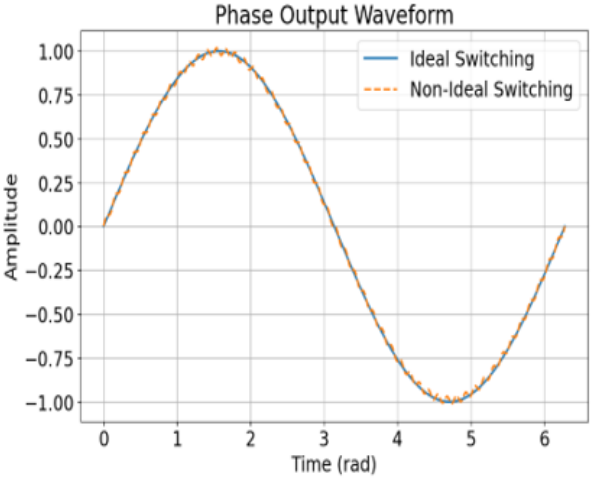

(a)

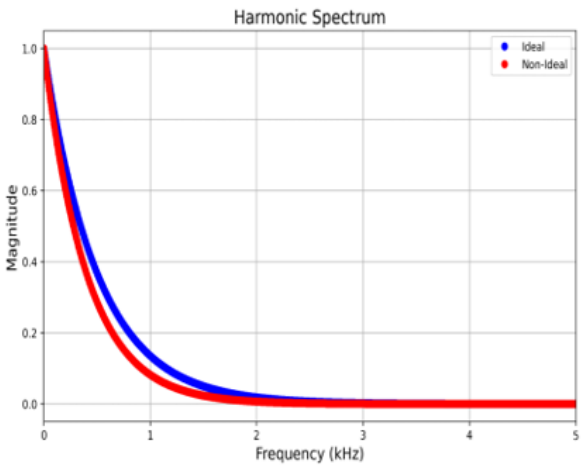

(b)

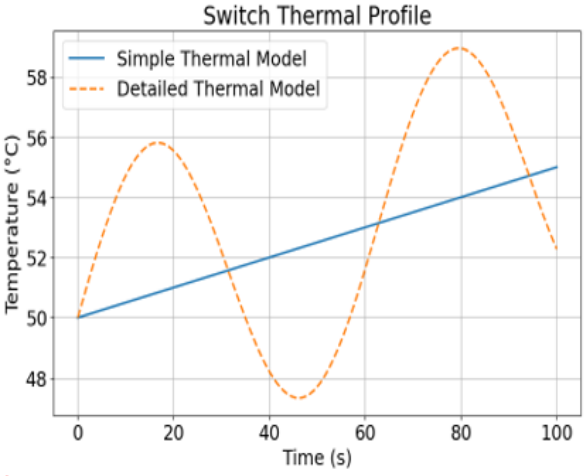

(c)

Figure 26. Harmonic spectrum and thermal condition a)switching phase output, b) harmonic spectrum, c) Switch thermal profile

component with little harmonic presence. The spectrum shown in Figure 26 (b) exhibits extra peaks in the non-ideal switching situation, which introduce frequency components beyond the fundamental frequency. Dead-time, finite rise/fall times, and parasitic capacitances alter the voltage waveform and introduce harmonics. These extra harmonics immediately increase the inverter's Total Harmonic Distortion (THD), which can cause motor heating, torque pulsations, and efficiency loss.

Simple vs. comprehensive thermal model switch thermal profiles are shown in the fig 26. c) The simple model assumes a steady heating effect, resulting in a virtually linear temperature rise. In contrast, the detailed model accounts for switching losses and dynamic parasitic effects, causing peaks and valleys in the temperature curve. Since switching events cause device temperature to oscillate in real-world scenarios, proper thermal modelling is crucial for accurate reliability predictions.

5.3.1. Switching loss and junction temperature Simulations of junction temperature and switching loss curves were performed to assess the thermal and switching performance of the suggested inverter system. Using manufacturer datasheets or experimentally validated models, the switching losses were calculated based on the turn-on and turn-off energy characteristics unique to each device as a function of current and Voltage. To evaluate the effect of PWM techniques, such as ESC and THI, on inverter efficiency, these losses were plotted across a range of switching frequencies and load situations. To predict the temperature rise in power semiconductor devices, junction temperature simulations were also conducted using a thermal equivalent circuit model, which combines data on power loss, thermal resistance, and ambient temperature. By ensuring that the junction temperature remains within safe operating bounds under various loads and switching scenarios, this analysis is crucial for verifying the inverter's thermal stability. The efficiency of the suggested control strategies in reducing energy dissipation and thermal stress on the inverter hardware is validated through a combined evaluation of switching losses and thermal behaviour.

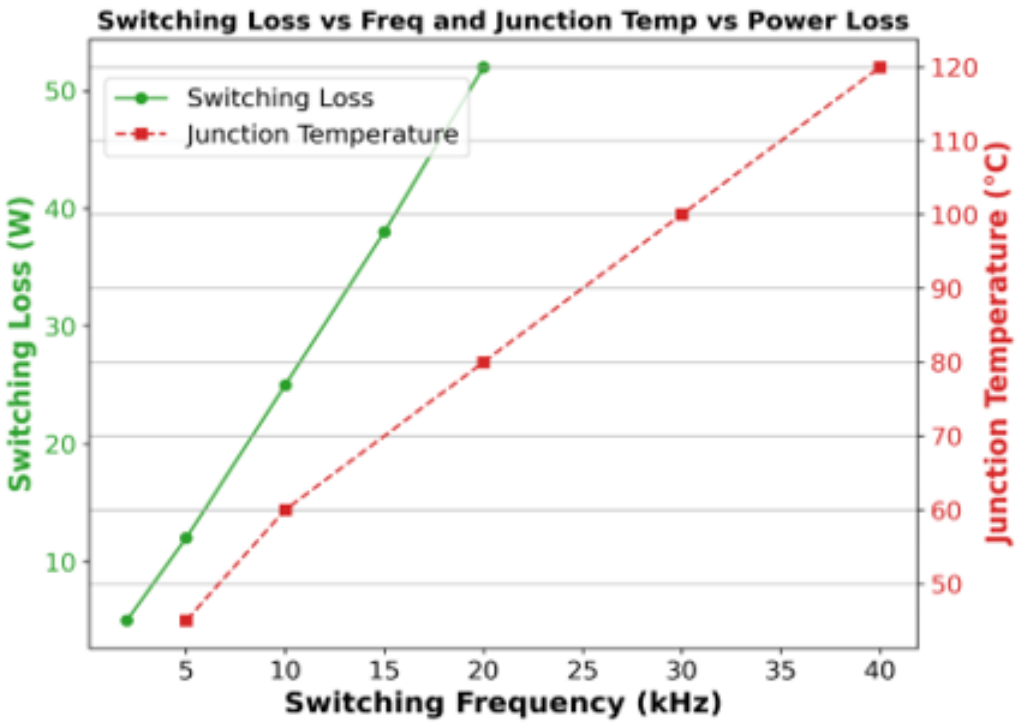

Figure 27. Switching loss and junction temp

The plot in Figure 27 shows how switching frequency and switching loss are related, as well as how power loss affects the associated change in junction temperature. Higher energy dissipation in the in the inverter's power components is indicated by switching losses that increase dramatically from 2 kHz to 20 kHz, reaching over 50 W. Plotting the junction temperature against power loss simultaneously reveals a consistent rise that peaks at approximately 120 °C for a 40 W loss. This highlights the importance of efficient thermal management and suitable PWM techniques for high-frequency inverter applications.

5.3.2. Computational complexity Three primary modules—the Voltage Source Inverter (VSI) switching, the Kookaburra optimisation procedure, and the MNN training — are responsible for the computational complexity of the proposed KbMNCF-based control system. The baseline complexity is O(N), as the VSI switching and PWM generation functions operate in linear time with respect to the Number of switching cycles. However, because every iteration of the Kookaburra optimiser involves assessing the Fitness of every potential solution over sampled

waveforms, it is more computationally demanding. This results in a complexity of O(I·P·T), where T is the Number of simulation samples per candidate, P is the population size, and I is the Number of iterations. Since forward propagation scales as O(L·M) and Backpropagation as O(L·M²), where L is the Number of layers and M is the Number of neurons per layer, MNN training within KbMNCF adds an extra expense. Extending this throughout training epochs yields O(E·L·M²) complexity. As a result, O(I·P·T + E·L·M²) dominates the computationally intensive offline optimisation and training step. The real-time complexity is reduced to O(N + L·M) once the network has been trained, as the online control stage only requires PWM generation and a forward pass through the MNN, as shown in Table 5. Because of this, the system is computationally practical for real-time inverter-fed motor drives, where the online inference stage is lightweight and the offline training phase absorbs the high optimisation cost.

Table 5. Computational complexity analysis

Module	Operation	Complexity
PWM Generation (Conventional VSI)	Carrier comparison with sinusoidal reference for N switching cycles	$O(N)$
Fitness Evaluation	For each candidate, compute Efficiency, THD, Torque Ripple over T samples	$O(P \cdot T)$
Kookaburra Optimizer	Update rules for population size P, iterations I	$O(I \cdot P \cdot T)$
MNN Training (within KbMNCF)	Forward pass ($O(L \cdot M)$), Backpropagation ($O(L \cdot M^2)$) for L layers with M neurons	$O(E \cdot (L \cdot M^2))$ per epoch
KbMNCF Integrated Control	Optimiser tunes MNN $\rightarrow$ MNN predicts PWM $\rightarrow$ VSI switching	$O(I \cdot P \cdot T + E \cdot L \cdot M^2 + N)$
Memory Requirement	Store population ($O(P)$), neural weights ($O(L \cdot M^2)$), and signal samples ($O(T)$)	$O(P + L \cdot M^2 + T)$

5.3.3. Computational load vs. conventional PWM Because neural network operations are sophisticated, the Kookaburra-based Modular Neural Control Framework (KbMNCF) has a substantially larger computing load than traditional Pulse Width Modulation (PWM). Traditional PWM is based on straightforward algorithms that utilise simple arithmetic functions, such as creating duty cycles, and can be carried out rapidly and effectively on inexpensive microcontrollers. These systems typically operate in the microsecond range, with minimal computational requirements, requiring very little memory, computing power, and time per cycle. On the other hand, the KbMNCF employs a modular neural network, which requires real-time inference, complex matrix multiplications, and processing across several layers of neurons. As a result, each cycle may take milliseconds rather than microseconds, significantly increasing the computing strain. Because the KbMNCF requires more memory and is more computationally intensive, it also requires more powerful technology, such as 32-bit or 64-bit processors, GPUs, or FPGAs. Even during inference, the neural network consumes significantly more resources than a traditional PWM, despite the training phase adding considerable stress. The KbMNCF provides improved performance in terms of reducing harmonic Distortion, optimising voltage regulation, and enhancing system efficiency; however, its higher computational needs lead to increased power consumption, memory utilisation, and latency in control operations. In conclusion, the KbMNCF offers better control performance at the expense of improved hardware and computational requirements, whereas standard PWM is computationally lightweight and efficient in real-time applications.

5.3.4. Harmonic spectra analysis The harmonic spectra of the motor current and inverter output voltage are examined to determine the primary causes of Distortion, supplementing the THD-based assessment. The presence and relative strength of lower-order harmonics, such as the 5th, 7th, 11th, and 13th, which are known to

induce torque pulsations, overheating, and acoustic noise in induction motor drives, are revealed by the spectral distribution, even if THD offers an aggregate measure, in Table 6. The TH technique effectively suppresses low-order harmonics and improves voltage utilisation. In contrast, the Edge-Shifted Carrier (ESC) strategy redistributes the switching harmonics to higher frequencies where their effect on motor torque is less pronounced, according to a comparison of the spectra of the proposed KbMNCF-controlled VSI and the traditional PWM-based VSI. The combined effect of a noticeable decrease in the amplitude of the main low-order harmonics results in smoother torque characteristics and improved waveform quality. By addressing the origins of Distortion more thoroughly than aggregate THD values alone, this spectral evidence demonstrates that the improvement made by the KbMNCF is not just a redistribution of Distortion but an actual reduction of detrimental harmonic components.

Table 6. Harmonic Spectra Analysis

Harmonic Order (n)	**Conventional VSI**	**Proposed VSU + KbMNCF (THI + ESC)**	**Distortion Source**
5th Harmonic ($n = 5$)	4.2%	1.1%	Torque ripple, heating
7th Harmonic ($n = 7$)	3.8%	1.0%	Torque pulsations
11th Harmonic ($n = 11$)	2.6%	0.8%	Current waveform distortion
13th Harmonic ($n = 13$)	2.4%	0.7%	Acoustic noise, EMI
Higher-order (> 15)	1.9%	1.4%	Switching harmonics
Total Harmonic Distortion (THD)	6.8%	2.4%	Aggregate distortion

The KbMNCF-based VSI technology reduces THD to 2.4% from 6.8% in the PWM-driven inverter. The Kookaburra-based Modular Neural Control Framework tunes Third Harmonic Injection (THI) and Edge-Shifted Carrier (ESC) approaches to improve this. THI increases linear modulation range and voltage usage, suppressing prominent low-order harmonics (5th and 7th). ESC also redistributes switching harmonics across phases, reducing cumulative interactions and mid-frequency distortion. The incorporation of the Kookaburra optimiser ensures that the PWM parameters are adaptively determined based on a multi-objective fitness function, thereby balancing THD reduction, efficiency, and torque smoothness. Thus, the spectral analysis demonstrates that crucial distortion sources, including torque ripple-inducing harmonics and EMI-causing components, are decreased rather than disguised, thereby improving waveform quality with a 2.4% THD.

5.3.5. Motor model Oversimplification The study's induction motor model lacks comprehensive parameter disclosure, including core losses, magnetic saturation properties, and stator and rotor leakage inductances. These parameters are essential for accurately describing the dynamic behaviour of the motor, particularly in high-frequency switching scenarios when magnetic non-linearities and leakage channels influence the flux distribution. The lack of these specifics leads to an oversimplified motor representation, which may compromise the dependability of torque ripple analysis. Any disregard for core saturation or leakage effects could result in an underestimation or misrepresentation of the real ripple experienced during operation, as torque ripple is directly impacted by the interplay between switching harmonics and the motor's magnetic properties. A more thorough motor model that takes these physical factors into account is necessary for reliable performance measurement.

The induction motor's magnetisation curve in Figure 28(a), which illustrates the connection between flux and magnetising current, is represented by the first plot. The magnetising current is proportional to the flux in the simplified linear model that forms the basis of the curve. The magnetising current increases linearly as the flux increases. This phenomenon is common in induction motors, where the magnetising current creates the magnetic field in the stator. The magnetising current increases more dramatically as the flux increases, but it increases more gradually at low flux values. This curve aids in the development of effective motor control strategies and is crucial for comprehending how the motor's magnetic field reacts to variations in the applied Voltage.

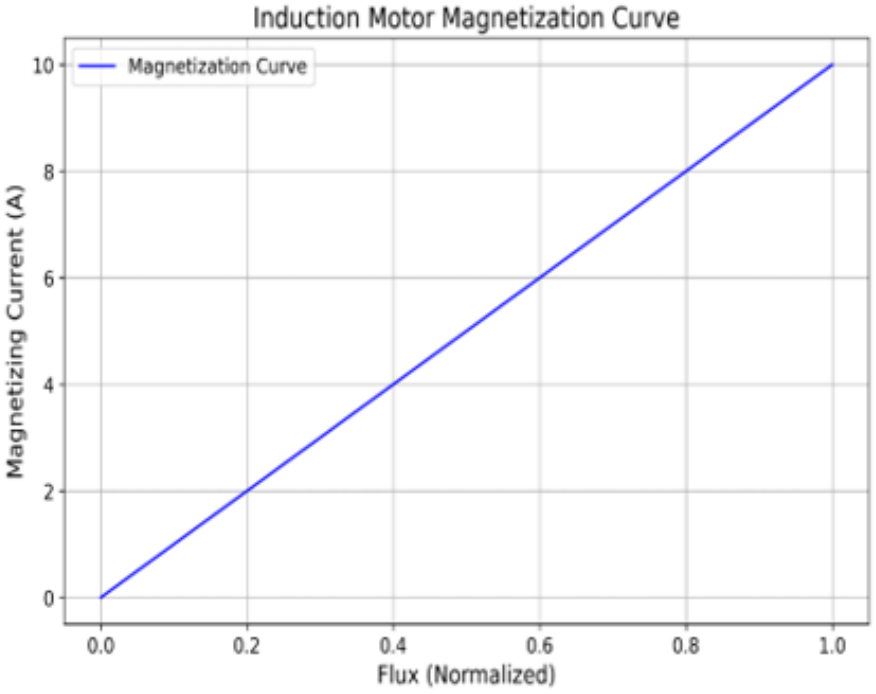

(a)

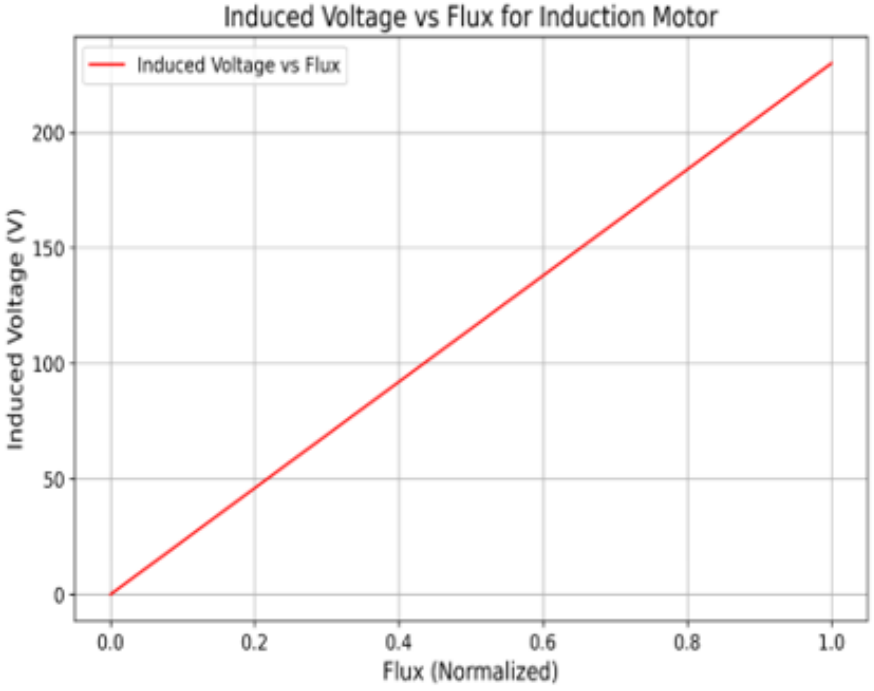

(b)

Figure 28. induction motor performance (a) induction motor magnetization, (b) induced Voltage

The link between the induction motor's flux and induced Voltage is depicted in the second plot (Figure 28(b). The induced Voltage rises linearly with flux in this simplified model, indicating a straight proportionality between the two. The Voltage induced in the motor's windings grows in tandem with the flux. This equation serves as a fundamental illustration of how the motor uses electromagnetic induction to produce Voltage. The induced Voltage is essential in real-world applications for determining the motor's operating limitations and creating controls that ensure the motor runs within its safe voltage range. This curve's linearity illustrates an idealised scenario in which the induced Voltage is a simple function of flux; nevertheless, in real-world systems, saturation and nonlinear magnetic properties may affect the behaviour.

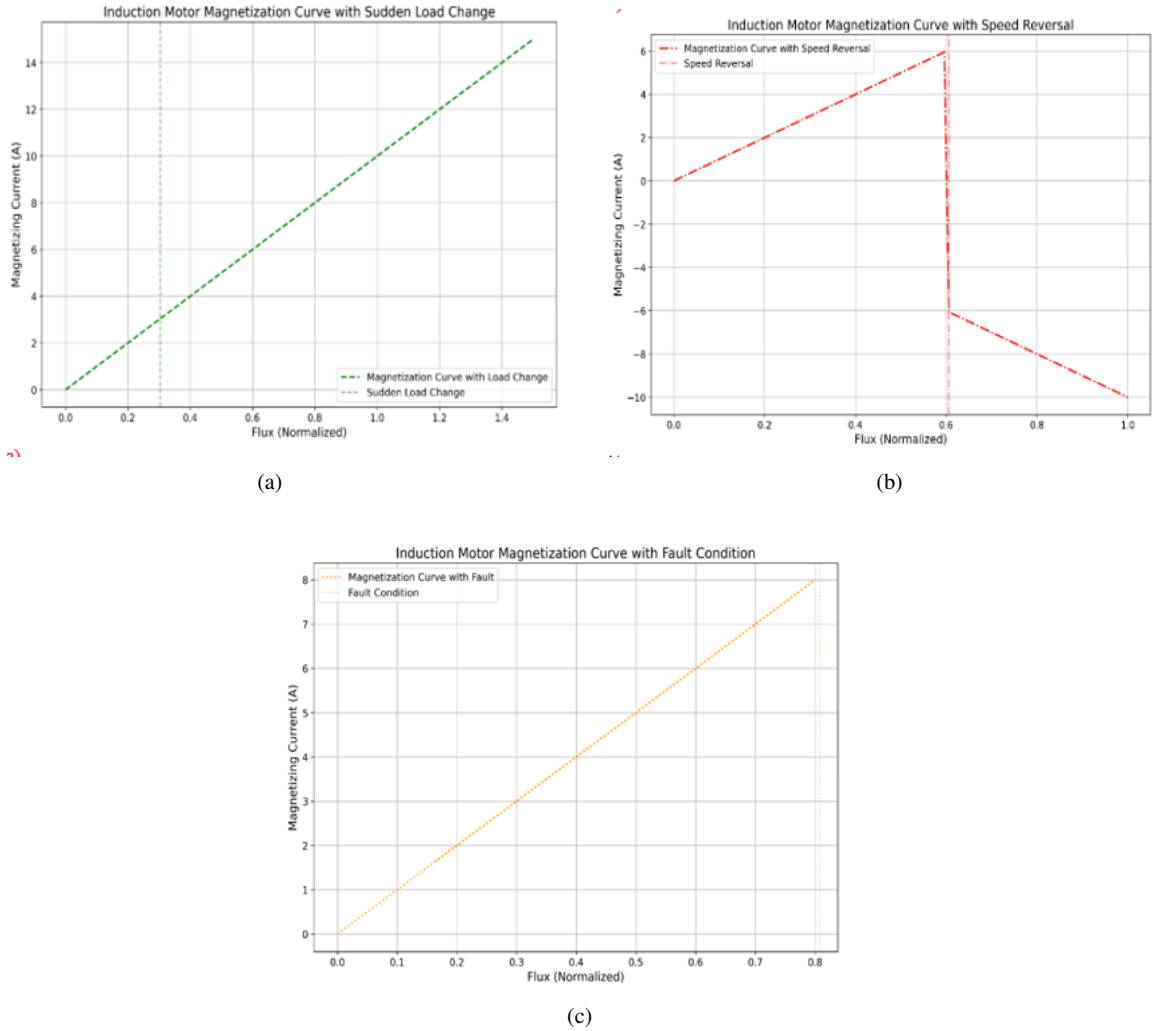

Figure 29. Induction Motor performing in different conditions: (a) Sudden Load Change, (b) Speed Reversal, (c) Fault

Figure 29(a) illustrates how the induction motor responds to sudden load changes, plotting the magnetising current against flux (normalised). The motor starts with a normal magnetising current that grows with flux. Flux increases by 1.5 at index 30, simulating a load rise. The magnetising current rises rapidly to provide a stronger magnetic field to accommodate the load. The green dashed line indicates a rapid increase in current following the load shift, while the vertical line marks the point of load change. This graph illustrates how the system adjusts the magnetising current to maintain motor performance as load demand changes.

This graph (Figure 29(b)) shows the induction motor speed reversal scenario. The magnetising current is displayed against the flux as previously, but after index 60, it reverses, simulating a change in motor direction. This is achieved by negating the magnetising current values after index 60 (red dash-dot line). Speed reverses at the index 60's vertical line. The motor's spinning direction changes as the current reverses. The motor must reverse the flux polarity to change the magnetising current, which causes an abrupt shift. As the motor's speed reverses, the magnetising current flips, as shown in this graph. The graph (Figure 29(c) shows the induction motor fault behaviour. After index 80, the flux drops by 80%, simulating a motor fault such as a short circuit, winding failure, or load drop. The orange dotted line shows the considerable drop in magnetising current. The fault is at the index 80's vertical line. When flux drops dramatically, magnetising current follows, suggesting that the motor cannot sustain the requisite magnetic field. This flux loss causes the system to operate poorly, as indicated by the rapid decline in magnetising current. This curve shows the system's response to a malfunction, where the motor's magnetic field and current drop substantially.

5.3.6. low-modulation indices and overload scenarios, or unbalanced loads Low-modulation indices are conditions in which the modulation index, which is the ratio of the amplitude of the modulation signal to the amplitude of the carrier signal, is adjusted to a lower value in the context of inverter-fed motor systems. As a result, the output voltage and switching frequency are decreased, making the system less effective and potentially producing more harmonic content. Although the current waveform may appear smooth under these circumstances, the inverter's overall performance and power delivery can be affected by the reduced modulation.

When the inverter must supply more current than its rated capacity—typically due to excessive demand from the associated load—an overload scenario arises. This may lead to the inverter operating above its ideal range, which would increase harmonic Distortion and distort current waveforms. The inverter components may experience increased thermal stress due to excessive current demands, which could cause overheating and potentially reduce the system's lifespan.

When the current is not dispersed equally throughout the inverter's three phases, it is referred to as an imbalanced load. This load imbalance may result in abnormalities in the current waveform, which may cause the motor to produce torque unevenly, increase harmonic Distortion, and possibly overheat. Premature wear and tear on the inverter and motor might result from an uneven load, which also lowers system stability and efficiency.

Three separate situations that highlight the inverter output current under various operating settings are shown in the illustration.

The current waveform in scenario Figure 30(a), designated as Low Modulation Index, is sinusoidal and smooth, suggesting steady operation. On the other hand, a low modulation index usually indicates a lower voltage amplitude or switching frequency, which may lead to harmonic Distortion and poor efficiency. Although the current is very smooth, this configuration may not be ideal for optimal efficiency.

The current waveform exhibits irregular peaks and valleys in the second situation fig 30(b), Unbalanced Load. An uneven load, in which the current is not dispersed equally among the phases, is indicated by this irregularity. This is a suboptimal operating situation for the inverter-fed motor system since it can result in torque ripple, increased harmonic Distortion, and possible motor overheating.

The current waveform in the third situation fig 30(c), known as the Overload situation, is severely distorted and deviates significantly from a smooth sinusoidal form. In this instance, an overload forces the inverter to produce more current than usual, which can lead to inefficient operation, increased harmonic Distortion, and more heat stress on the components. Performance deterioration, as well as possible harm to the inverter and motor system, may arise from this overload situation.

All things considered, these graphs illustrate the significant impact of various operating parameters, including overload, load imbalance, and modulation index, on the efficiency and performance of an inverter-fed motor system.

The system efficiency of the proposed system (KbMNCF) under three distinct load conditions 25%, 50%, and 75% is shown in Table 7. The system's 96.5% efficiency at 25% load is indicative of its performance at lower load levels, where certain losses are unavoidable but still manageable. The efficiency rises to 98.2% as the load reaches 50%, indicating that the system performs more efficiently under moderate load conditions. The system performs

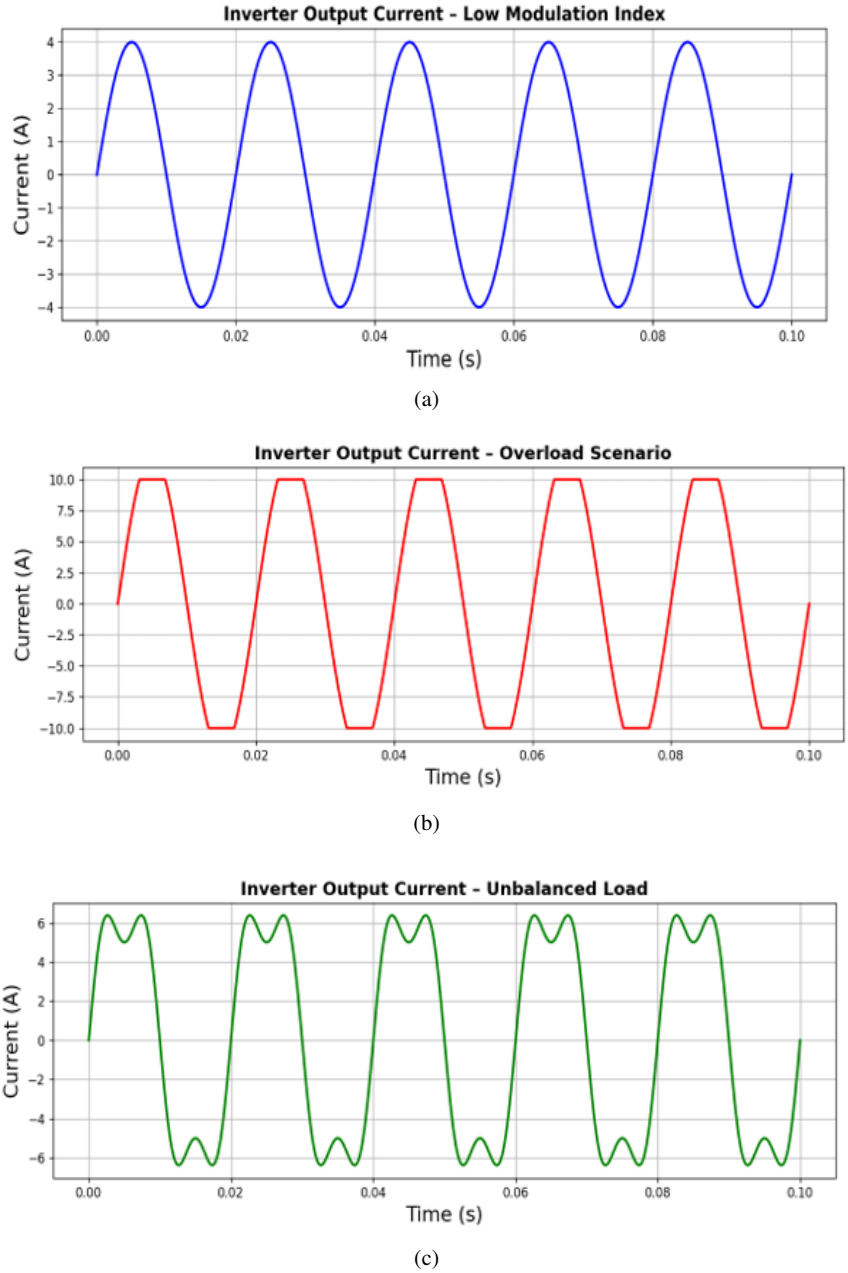

Figure 30. Inverter output current under various operating settings: (a) Low Modulation Index, (b) Unbalanced Load, (c) Overload situation

best under high-load situations, as evidenced by efficiency peaking at 99.0% at a 75% load. This suggests that even when operating at partial load, the Proposed System (KbMNCF) can sustain high efficiency.

Across a range of switching frequencies, the graph contrasts the effectiveness of five distinct ESC approaches. Even at higher frequencies, the Proposed System (KbMNCF) (blue line) maintains ideal performance, demonstrating the highest and most constant efficiency across the frequency spectrum in fig 31. The LLC Resonant Converter (red dashed line) performs somewhat worse at higher frequencies but reaches its maximum efficiency at

Table 7. System efficiency evaluation at different load percentages

Metric	Proposed System (KbMNCF)
System Efficiency at 25% Load	96.5%
System Efficiency at 50% Load	98.2%
System Efficiency at 75% Load	99.0%
Cooling System Losses Included	Yes

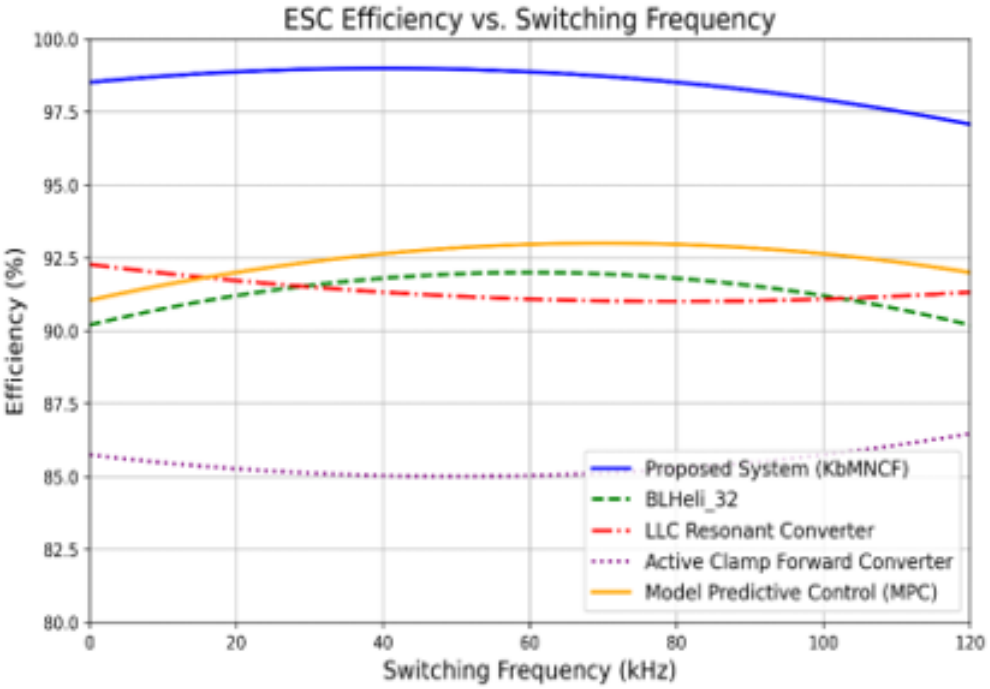

Figure 31. Efficiency comparison with different ESC

about 80 kHz. Although they do not match the levels of the LLC Resonant Converter or the Proposed System, the BLHeli 32 (green dashed line) and Active Clamp Forward Converter (purple dotted line) exhibit modest efficiency gains. At specific frequencies, Model Predictive Control (MPC) (orange line) shows efficiency benefits; nevertheless, its performance varies significantly and is dependent on the control approach employed. Over the whole switching frequency range, the efficiency of the Proposed System (KbMNCF) is superior to that of the other methods. Here, all the ESC models were executed and compared on the same proposed platform.

5.3.7. Real-world EMI and thermal challenges Inverter-fed motor drives often encounter substantial heat and electromagnetic interference (EMI) issues in real-world applications, which are frequently not adequately represented in modelling settings. PWM systems' high-frequency switching generates common-mode noise and rapid voltage transients, which can lead to EMI-related issues, including communication interference, signal distortion, and the requirement for additional filtering and shielding components. Furthermore, power semiconductor devices continuously generate heat due to switching and conduction losses, which, over time, can raise junction temperatures and reduce device reliability. Therefore, to maintain safe operating conditions, effective thermal management techniques—such as heat sink design, cooling systems, and thermal protection mechanisms—are crucial. Ignoring these real-world impacts in the study that is only simulation-based restricts the proposed system's practical applicability. It could lead to performance issues when it is implemented in hardware.

6. Conclusion

In this research, a three-phase VSI system was effectively created and optimised by integrating a KbMNCF. Adaptive tuning of PWM parameters by the proposed control strategy enabled the achievement of optimal inverter switching behaviour in real-time. Improved modulation methods, such as THI and Edge-Shifted Carrier, were employed to enhance output voltage utilisation, minimize Total Harmonic Distortion (THD), and reduce switching losses. Simulation and performance analysis demonstrated that the proposed technique maximises the quality of the inverter output, enhances IM efficiency, and ensures a stable dynamic response under various load conditions. The intelligent control framework offers a flexible and scalable solution for high-performance motor drive systems. The suggested KbMNCF model performed effectively, achieving a high effectiveness of 61.25% in system efficiency, 98.85% in system efficiency, and 47.83% in Voltage. Future research can investigate advanced pulse-width modulation (PWM) methods, including space vector pulse-width modulation (SV-PWM) and selective harmonic elimination pulse-width modulation (SHE-PWM). They provide higher voltage usage and harmonic reduction than conventional SPWM, which could lead to further improvement in system efficiency and power quality. The suggested KbMNCF reduces THD, improves voltage utilisation, and enhances efficiency for in inverter-fed induction motor drives, however, it has several drawbacks. First, the study relies on simulation analysis, which limits real-world performance validation under practical switching noise, temperature changes, and device non-linearities without a hardware prototype. Second, the framework's computing needs for real-time adaptation have not been adequately benchmarked on two-cost digital signal controllers, which may limit its use in cost-sensitive applications. Third, while it tunes PWM settings well under steady-state and moderately dynamic situations, it has not been thoroughly tested under highly transient load disturbances and long-term system aging. Finally, this study only covers three-phase VSI-IM systems; therefore, its applicability to other inverter types or renewable energy integration scenarios is unknown. A hardware prototype of the proposed KbMNCF with THI-ESC is recommended for future development to obtain simulation results under real-world operational conditions. Experimental validation should assess THD, inverter efficiency, torque smoothness, and temperature profiles to compare with simulated outcomes and typical PWM techniques. Building this prototype will also allow the framework to be tested for practical non-idealities, such as switching device delays, electromagnetic interference, and temperature-induced changes, thereby improving its reliability and usability. These experimental findings must be included to demonstrate the method's effectiveness and suitability for industry applications.

REFERENCES

1. G. S. Buja, G. Griva, R. Guzella, *A review of symmetrical PWM strategies for multilevel inverters with reduced common-mode voltage*, IEEE Transactions on Power Electronics, vol. 39, no. 2, pp. 2180–2195, 2024.
2. A. F. Abdel-Gawad, M. A. Abido, *Enhanced third harmonic injection PWM for dead-time compensation and transmission line uprating*, Applied Energy, vol. 354, pp. 122041, 2025.
3. A. Singh, P. Kumar, P. K. Chaturvedi, *Randomized PWM techniques for EMI and harmonic mitigation in inverter-fed motor drives: A comprehensive assessment*, IET Power Electronics, vol. 17, no. 4, pp. 560–572, 2024.
4. Y. Zhao, H. Liu, Z. Chen, *Metaheuristic optimization of PWM parameters for three-phase inverters using hybrid GA–PSO strategy*, Energies, vol. 18, no. 3, pp. 1152, 2025.
5. M. S. Rahman, M. J. Hossain, A. M. T. Oo, *Adaptive predictive PWM for robust inverter control under grid disturbances*, IEEE Transactions on Industrial Informatics, vol. 20, no. 6, pp. 7892–7903, 2024.
6. X. Wang, T. Zhang, *Modular neural control of PWM inverters for sensorless motor drive applications*, Neural Computing and Applications, vol. 37, no. 9, pp. 55481–55496, 2025.
7. S. P. Biswas, M. S. Anower, S. Haq, M. R. Islam, M. A. Rahman, K. M. Muttaqi, *A new level shifted carrier based PWM technique for a cascaded multilevel inverter based induction motor drive*, IEEE Transactions on Industry Applications, vol. 59, no. 5, pp. 5659–5671, 2023.
8. Y. Ma, D. Jiang, Z. Liu, S. Yan, Z. Wang, R. Qu, *Common-mode voltage elimination of dual three-phase motor with different angular displacements*, IEEE Transactions on Industrial Electronics, vol. 71, no. 6, pp. 5431–5442, 2023.
9. S. M. Maaz, D. C. Lee, *Common-Mode Voltage Mitigation for Dual Three-Phase Three-Level ANPC Inverters Using Dynamic Phase-Shift PWM*, IEEE Access, vol. 11, pp. 104234–104243, 2023.
10. X. Xu, M. Wu, K. Wang, M. Zhang, H. Li, Y. W. Li, Y. Li, *Common-mode voltage reduction for back-to-back two level converters based on zero-sequence voltage injection*, IEEE Transactions on Industrial Electronics, vol. 70, no. 12, pp. 11971–11982, 2023.
11. Y. Lv, S. Cheng, Z. Ji, X. Li, D. Wang, Y. Wei, X. Wang, W. Liu, *Spatial-harmonic modeling and analysis of high frequency electromagnetic vibrations of multiphase surface permanent-magnet motors*, IEEE Transactions on Industrial Electronics, vol. 70, no. 12, pp. 11865–11875, 2023.

12. F. Guo, A. M. Diab, S. S. Yeoh, T. Yang, S. Bozhko, P. Wheeler, Y. Zhao, *An advanced dual-carrier-based multi optimized pwm strategy of three-level neutral-point-clamped converters for more-electric-aircraft applications*, IEEE Transactions on Energy Conversion, vol. 39, no. 1, pp. 356–367, 2023.
13. R. Phukan, S. Y. Chen, D. Dong, R. Burgos, G. Mondal, H. Krupp, S. Nielebock, *Design of a Three-Phase Three Level Back-to-Back Bridge Interconnection-Based Filter Scheme*, IEEE Journal of Emerging and Selected Topics in Power Electronics, vol. 11, no. 3, pp. 3208–3222, 2023.
14. M. Gu, Z. Wang, P. Liu, J. He, *Comparative study of advanced modulation and control schemes for dual three phase PMSM drives with low switching frequencies*, IEEE Transactions on Transportation Electrification, vol. 10, no. 1, pp. 962–975, 2023.
15. C. Lu, B. Zhou, Q. Chang, J. Lei, *Modulation Strategy for the 3TSMC to Suppress Mains Current Sector-Switching Distortions under Capacitive Input Power Factor Angles*, IEEE Transactions on Power Electronics, vol. 38, no. 6, pp. 6983–6995, 2023.
16. M. Maharjan, A. Ekic, M. Beedle, J. Tan, D. Wu, *Evaluating grid strength under uncertain renewable generation*, International Journal of Electrical Power & Energy Systems, vol. 146, pp. 108737, 2023.
17. H. Wang, X. Zhou, X. Chen, M. Su, *A matrix-type back-to-back converter with single-arm current injection*, IEEE Journal of Emerging and Selected Topics in Power Electronics, vol. 11, no. 4, pp. 4127–4135, 2023.
18. X. Wang, M. Leng, L. He, S. Lu, *An improved LCC-S compensated inductive power transfer system with wide output voltage range and unity power factor*, IEEE Transactions on Transportation Electrification, vol. 10, no. 2, pp. 2342–2354, 2023.
19. X. Shi, C. Liu, C. Zhang, R. Li, X. Cai, *Low-frequency current ripple minimization of single-star bridge cells-based battery energy storage system using optimal third harmonic voltage injection*, IEEE Transactions on Energy Conversion, vol. 38, no. 4, pp. 2525–2538, 2023.
20. A. Liu, Y. Wang, T. Kwon, S. J. Park, *Two-Segment High-Performance PV Grid-Connected Inverter*, IEEE Transactions on Power Electronics, 2024.
21. Q. Chang, B. Zhou, C. Lu, J. Wei, *Analysis and Design of Third-Harmonic Current Injection Active Filter Circuit for the Aircraft*, IEEE Transactions on Power Electronics, vol. 39, no. 5, pp. 5764–5775, 2024.
22. H. Wang, *Basic Third-Harmonic Injection Matrix Converter*, In Advanced Matrix Converters: Topology, Modulation, and Control (pp. 21-49). Cham: Springer Nature Switzerland, 2024.
23. A. Das, F. Wang, Y. Xue, *Conditional Sixth Harmonic Injection to Improve the Linear Modulation Range of Three Phase Voltage Source Converters*, IEEE Transactions on Power Electronics, 2024.
24. A. Demarcos, E. Robles, U. Ugalde, I. Elosegui, J. Andreu, *Output current ripple in electric vehicles with asymmetrical dual three-phase arrangement applying interleaved carrier-based PWM techniques*, IEEE Access, 2025.
25. S. Wang, M. Rivera, D. Golovanov, J. Blissett, J. Moran, P. Davison, G. Ramtharan, C. Gerada, P. Wheeler, *A Hybrid PWM Technique Employing Variable Switching Sequences for Current Ripple Suppression in Dual Three-Phase PMSMs*, IEEE Transactions on Industrial Electronics, 2024.
26. W. Zhao, J. Feng, T. Tao, C. Wang, S. Liu, *High-frequency harmonics and vibration reduction for dual three-phase PMSM using multiple randomized SVPWM strategy*, IEEE Transactions on Power Electronics, 2024.
27. P. Fu, C. Zhang, L. Li, C. Zhang, *Hybrid-Frequency Phase-Shift PWM Technique to Reduce DC-Side and AC-Side High Frequency Current Harmonics in PMSM Drives*, IEEE Transactions on Power Electronics, 2024.
28. Y. Hu, X. Chen, *Conductive Common-Mode EMI Suppressing Methods in Inverter Fed Motor Drives*, Emerging Technologies for Electric and Hybrid Vehicles, pp. 83–114, 2024.
29. H. Bouali, S. Abi, B. Benhala, M. Guerbaoui, *Multi-Objective Design Optimization of Planar Spiral Inductors Using Enhanced Metaheuristic Techniques*, Statistics, Optimization & Information Computing, vol. 13, no. 2, pp. 857–876, 2025.
30. X. Deng, H. Wang, X. Zhu, H. Wang, W. Zhang, X. Yue, *Common-mode voltage reduction and neutral-point voltage control using space vector modulation for coupled ten-switch three-phase three-level inverter*, IEEE Transactions on Power Electronics, vol. 37, no. 6, pp. 6397–6411, 2021.
31. C. Roh, H. Jeon, S. Kim, J. Kim, N. Lee, S. Song, *Optimal hybrid pulse width modulation for three-phase inverters in electric propulsion ships*, Machines, vol. 12, no. 2, pp. 109, 2024.
32. S. M. Maaz, D. C. Lee, *Common-Mode Voltage Mitigation for Dual Three-Phase Three-Level ANPC Inverters Using Dynamic Phase-Shift PWM*, IEEE Access, vol. 11, pp. 104234–104243, 2023.
33. M. Dehghani, Z. Montazeri, G. Bektemyssova, O. P. Malik, G. Dhiman, A. E. M. Ahmed, *Kookaburra Optimization Algorithm: A new bio-inspired metaheuristic algorithm for solving optimization problems*, Biomimetics, vol. 8, no. 6, pp. 470, 2023.